This project has received funding from the European Union's Seventh Programme for research, technological development and demonstration under grant agreement No [308417]".

New Directions in Seismic Hazard Assessment through Focused Earth Observation in the Marmara Supersite

Grant Agreement Number: 308417
co-funded by the European Commission within the Seventh Framework Programme
THEME [ENV.2012.6.4-2]
[Long-term monitoring experiment in geologically active regions of Europe prone to natural hazards: the Supersite concept]

D6.1

Report on local instability areas and advanced susceptibility mapping for on-shore landslides

Project Start Date	1 November 2012
Project Duration	36 months
Project Coordinator /Organization	Nurcan Meral Özel / KOERI
Work Package Number	WP6
Deliverable Name/ Number	Report on local instability areas and advances susceptibility mapping for on-shore landslides-D6.1
Due Date Of Deliverable	Month 24
Actual Submission Date	24/03/2015
Organization/Author (s)	INERIS/P. BIGARRE

Dissemination Level		
PU	Public	
PP	Restricted to other programme participants (including the Commission)	
RE	Restricted to a group specified by the consortium (including the Commission)	
CO	Confidential, only for members of the consortium (including the Commission)	

TABLE OF CONTENTS

1 INTRODUCTION

1.1 MARSITE WP6

Earthquake-triggered landslides have an increasing disastrous impact in seismic regions due to the fast growing urbanization and infrastructures. Just considering disasters from the last fifteen years, among which the 1999 Chi-Chi earthquake, the 2008 Wenchuan earthquake, and the 2011 Tohoku earthquake, these events generated tens of thousands of coseismic landslides. Those resulted in amazing death toll and considerable damages, affecting the regional landscape including its hydrological main features.

Despite a strong impetus in research during past decades, knowledge on those geohazards is still fragmentary, while databases of high quality observational data are lacking. These phenomena call for further collaborative researches aiming eventually to enhance preparedness and crisis management.

As one of the three SUPERSITE concept FP7 projects dealing with long term high level monitoring of major natural hazards at the European level, the MARSITE project gathers research groups in a comprehensive monitoring activity developed in the Sea of Marmara Region, one of the most densely populated parts of Europe and rated at high seismic risk level since the 1999 Izmit and Duzce devastating earthquakes.

Besides the seismic threat, landslides in Turkey and in this region constitute an important source of loss. The 1999 Earthquake caused extensive landslides while tsunami effects were observed during the post-event surveys in several places along the coasts of the Izmit bay.

The 6th Work Package of MARSITE project gathers 9 research groups to study earthquake-induced landslides focusing on two sub-regional areas of high interest. First, the Cekmece-Avcilar peninsula, located westwards of Istanbul, is a highly urbanized concentrated landslide prone area, showing high susceptibility to both rainfalls while affected by very significant seismic site effects. Second, the off-shore entrance of the Izmit Gulf, close to the termination of the surface rupture of the 1999 earthquake, that shows an important slump mass facing the Istanbul coastline.

A multidisciplinary research program based on pre-existing studies has been designed with objectives and tasks linked to constrain and tackle progressively some challenging issues related to data integration, modeling, monitoring and mapping technologies.

Concerning the on-shore area, this program includes the refined analysis of the seismic site response, the permanent multi-parameter ground monitoring of a representative unstable slope as well as the in-depth slope stability analysis based on the stress-strain dynamic numerical modelling approach. Hyperspectral and Dinsar imagery technologies are also deployed to complete inventory and observational information. The development of a dynamic GIS tool featuring capabilities to integrate and process very different types of data, and up-date susceptibility maps based on near to real-time rainfall-seismic shaking input, is currently undertaken. Moreover, the research is gaining high profit of a vast drilling program undertaken by the Istanbul Metropolitan Area, aiming to yield a detailed geological and geotechnical characterization of the slopes. Also included in the objectives is to test a landslide early warning system.

As regards the selected off-shore area, high resolution geophysical marine surveys are being conducted to complete its geomorphological description to help in mapping possible incipient mass movements. This is especially expected to provide better-constrained input for both laboratory testing and numerical modeling of tsunami scenarios thank to a unique lab-scale tsunami channel.

Recall that the 6th Work Package of MARSITE FP7 project gathers 9 research groups (INERIS, IU, ITU, TUBITAK, INGV, CNR, University of Pavia, IFSTTAR - University of “La Sapienza”)

to study earthquake-induced landslides, focusing on the survey and monitoring of two sub-regional areas of high interest. The research aims to improve the preparedness of those seismically induced landslide geohazards, through the using of surveying, modelling and monitoring approaches.

First, on the on-shore side, the Cekmece-Avcilar peninsula located westwards of Istanbul, was selected as a highly urbanized concentrated landslide prone area, showing high susceptibility to both landslide and liquefaction phenomena (Duman et al., 2005). This area is the object of onshore studies for tasks 1b and 2b, and the first results of the undertaken work studies will be showed in this deliverable and in the deliverable D 6.3.

Second, the off-shore entrance of the Izmit Gulf was selected, close to the termination of the surface rupture of the 1999 earthquake that shows an important slump mass facing the Istanbul coastline. This area is the object of analyses for tasks 1a and 2a, and the results of these studies will be showed in the deliverables D6.2 and D6.3.

This deliverable summarizes the multidisciplinary scientific contribution realized in the task 1b (on-shore landslides). The work subdivision for this task was the following:

- Geological data recovery and sharing by **TUBITAK**.
- Identification and characterization of gravitational phenomena with photogeological interpretation and analysis of ENVISAT-ERS DInSAR temporal series by **INGV**.
- Evaluation of the resolution and identification of landslide hazard-related features using space multispectral/hyperspectral image data by University of Pavia (**UNIPV**).
- Identification of an active landslide, through different field surveys, as a potential pilot site by INERIS, TUBITAK , IU and **IFSTTAR & CERI-Sapienza**. This pilot site was instrumented in the frawework of the WP9.
- Development of landslide hazard map and associated uncertainties with a dynamic GIS approach aiming to integrate strong ground motion, intense and/or prolonged rainfall as a potential worsening factor during seismic shaking and instrumentation of this pilot site with an in situ multi-parameter observational system, including displacement, rainfall and seismic shaking measurement by **INERIS**.

1.2 IBB Project

Moreover, the undertaken research in WP6 is gaining high profit of a vast drilling program (*IBB project*) undertaken by the Istanbul Metropolitan Area, aiming to yield a detailed geological and geotechnical characterization of the slopes throughout the west part of the Cekmece-Avcilar peninsula. Thanks to the TUBITAK partner it was possible to benefit of some of the important results of this field investigation program in this European project and, moreover, to use one borehole to set up a local seismic observational network on a very slow massive landslide (so-called on shore pilot site).

2 OVERVIEW OF THE ON-SHORE AVCILAR LANDSLIDE PRONE AREA

The on-shore area of interest locates at the northern coast of the Sea of Marmara and western part of Istanbul metropolitan city (Figure 1). The active northern branch of the North Anatolian Fault Zone (NAFZ) passes through approximately 10-km from south of the studied site. Recall that in the last decade, the region of Marmara has experienced some large earthquakes and more than 300 earthquakes in the region have been reported to have occurred between 2100 BC and AD 1900. In the last 20 centuries, between Izmit and Gulf of Saros, 29 historically large earthquakes occurred along the northern branch of the NAFZ (Figure 2).

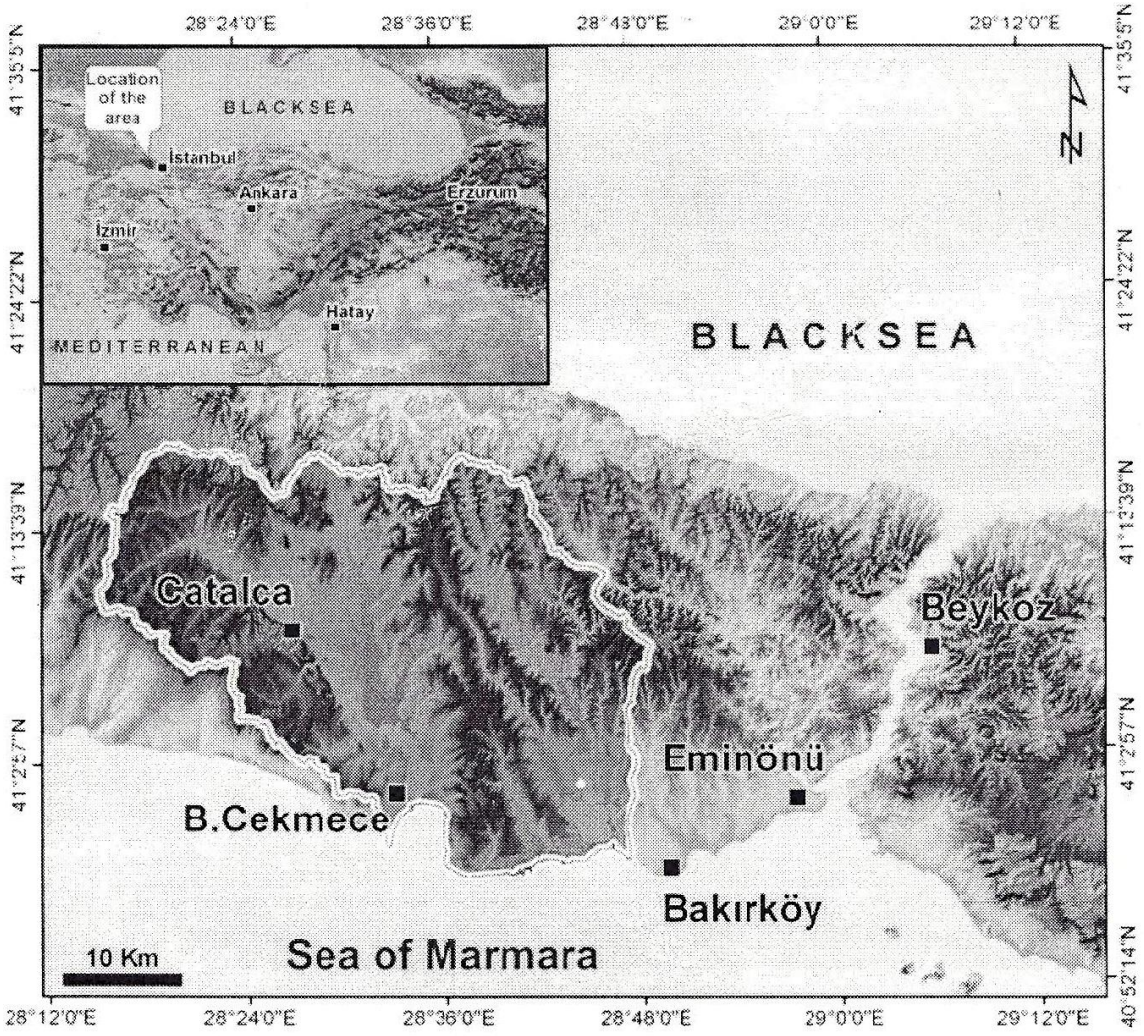

Figure 1: Location map of the site. While outlined zone denotes the outer-boundary of the high landslide density area.

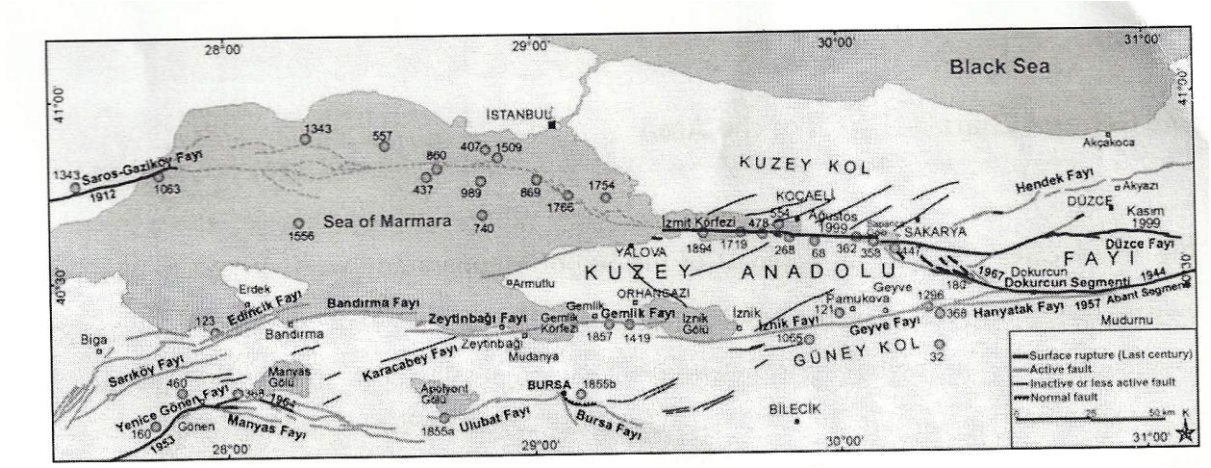

Figure 2: Active faults and historical earthquakes around the sea of Marmara (MTA, 2011).

2.1 Meteorological setting

In the area of interest, summers are characterized by hot and slightly rainy periods while winters are warm and generally rainy. The topography of the region and presence of lakes and dams also affect the local climatic conditions (http://istanbul.meteor.gov.tr). The region receives 85% of the annual precipitation in the period of September-May (http://istanbul.meteor.gov.tr) and the average monthly rainfall varies between 20-mm and 102-mm. The annual precipitation varies between 500-mm and 1000-mm in the region while average annual precipitation of long period of the Florya Meteorology Station is 640-mm. The maximum daily precipitation was observed in Istanbul as 89-kg/m² (http://meteo.gov.tr). The precipitation is highly effective on the landslide occurrence in the area.

2.2 Geological setting

Geologically, the study area is covered by Oligo-Miocene aged lithological formations and Quaternary aged cover units. Stratigraphically, Oligocene aged Cukurcesme formation is the oldest rocks between the Küçükçekmece and Büyükçekmece lakes and is observed in the eastern and western sides of the lakes (Figure 3). In this formation the dominant lithology is grayish green clay of high plasticity, over consolidated and of stiff to hard consistency (Ince, et al., 2008; Yildirim and Savaskan, 2003). The stratigraphic sequence continues with clay and marl, interbedded with limestone and sand lenses of the Upper Miocene aged Gungören formation. This formation is composed of black-dark grey clay of high plasticity with a considerable organic content and swelling potential (Sayar, 1977). The Late Miocene aged Bakirköy formation consists of limestones and claystones, and crops out central parts of the area (Figure 3). This formation is composed of lacustrine, off-white-cream colored, flat-bedded, moderately strong Mactra bearing limestone and weak to moderately strong marl, usually interbedded with green clays (Ince, et al., 2008; Yildirim and Savaskan, 2003; Özgül, 2005) The youngest units in the study area are Quaternary aged alluviums and landslide deposits. These units are unconformably overlain the oldest rocks along the eastern and western margins of Büyükçekmece and Küçükçekmece lakes, respectively. In the area, presences of some inactive faults have been revealed through geophysical surveys and geological observations (Koral, 1998; Yurtsever and Caglayan, 2002; Gokasan et al., 20013; Duman et al., 2004 and 2005; Sen, 2008).

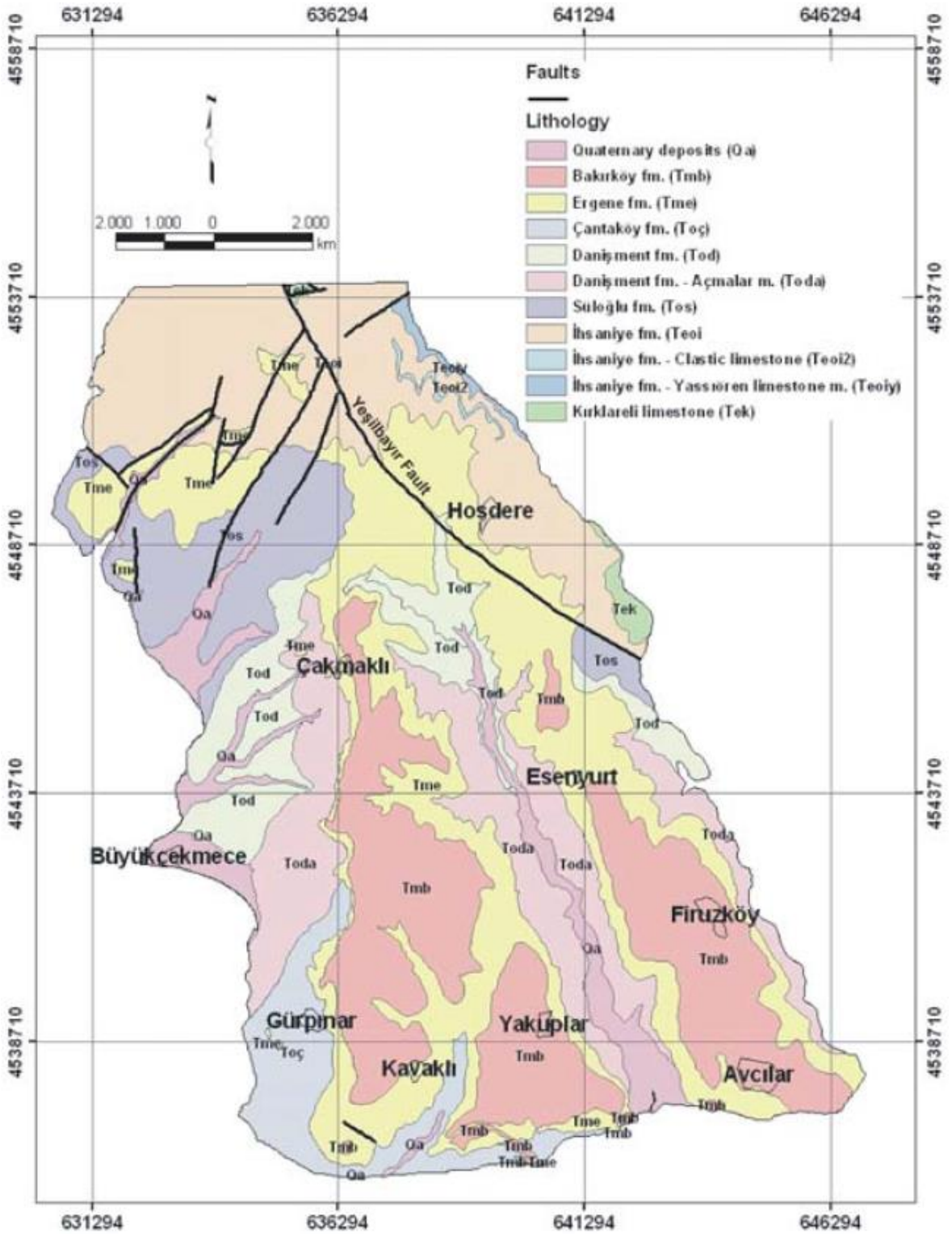

Figure 3 : Geological map of the area (from Duman et al., 2004)

These fault's trend is generally northwest-southeast direction and mostly semi-parallel to the eastern and the western costs of the Çekmece lakes. The dips of the sedimentary units in the area are rather low, 5-15° and show a high variation over short distances (Duman et al., 2005 and 2006).

2.3 Landslide distribution, characteristics and potential triggering factors in the area

The majority of landslides in the region cluster between Küçükçekmece and Büyükçekmece lakes (Figure 4). Most of these landslides, except two small landslides in the clay levels of the Pliocene at the western side of the Küçükçekmece bay, occurred on the clay and varve bearing levels of the Gürpinar formation.

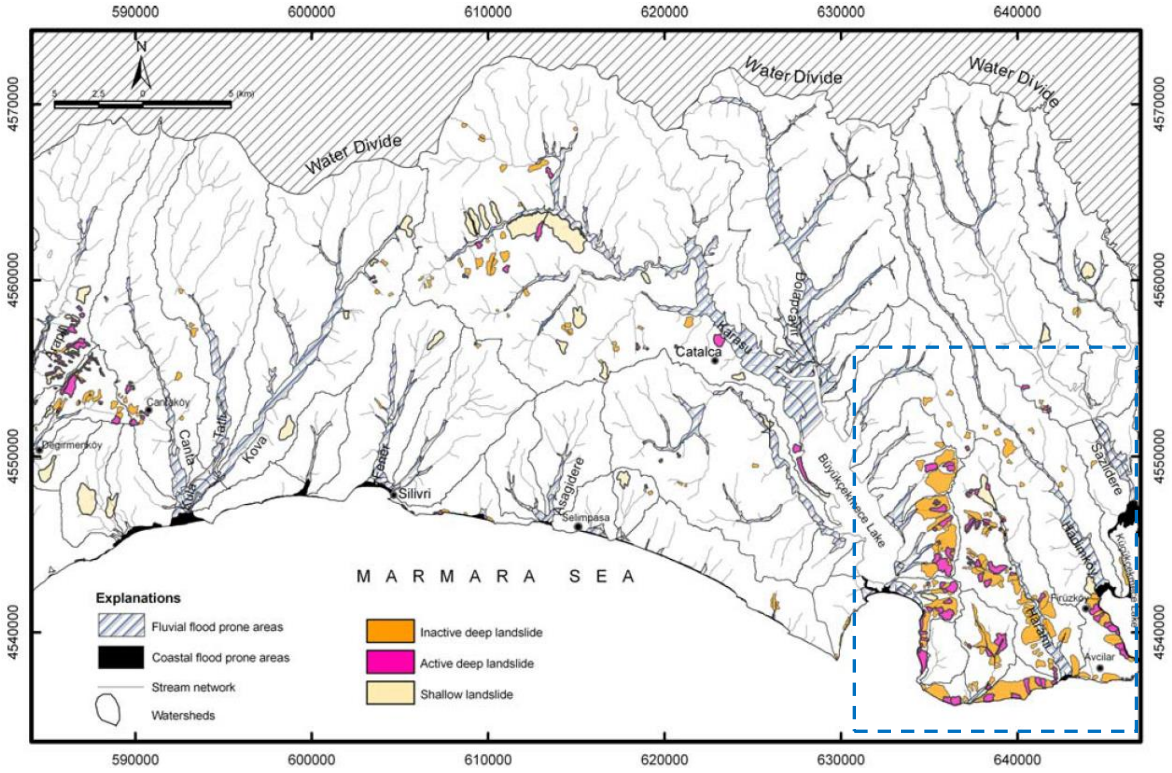

Figure 4: Landslide distribution map of the area (from Duman et al., 2005)

The types of landslides generally occurring in this area are deep seated translational debris, rock slides, shallow slides and flows. Their surface areas changes from 0.005-km2 to 2.0-km2 and most of them are inactive nowadays. In general, the scarp sections of the landslides are apparent but the toe sections of the landslides are not very apparent. The reason for this is the presence of erosion resistant clay and sand bearing sections of the Çukurçeşme formation at the locations of scarp sections of the landslides.

It is thought that the changing slope gradient conditions due to the incision of the rivers, which has increased their erosional activities due to sea level changes in Pleistocene, have been effective on the hillslope instabilities (Arpat, 1999). Nowadays, the landslides are occurring from the reactivation of the old landslides. Residual shear strength of these landslides is quite small (<12°). Besides the deep-seated landslides with very low velocities, there have been also highly damaging earth flows with relatively high velocity in the region. These earth flows are mostly effective in the east coasts of Büyükçekmece (Figure 5).

Litho-stratigraphic characteristics of the region is the most important factor controlling the distribution and density of the landslides in the region. Heavy rains with 10 years of return period and also human activities (i.e. 2004 Veryant landslide near ISKI water pump station in Büyükçekmece) are known to be among the landslides triggering factors. Moreover, although there is no historical record, the earthquakes can also be considered as a potential triggering factor for the landslides on the region.

The settlements in these areas have been adversely affected by the landslides. Landslides are highly typical along the riversides of Harami and Kalyos streams, between Beylikdüzü and Kirac

villages, and between the Küçükçekmece lake and Firüzöy (Figure 5 and Figure 6). Landslides in these districts also cause economic losses. The housing development consisting of apartment blocks in the southern part of the Gürpinal district was considerably affected by the landslides. In addition, some settlements in high landslide risk areas near Ambarli district (Avcilar) were evacuated (Figure 7).

Figure 5: Recent activities of Firüzköy landslide and Büyükçekmece earthflow after heavy rains on 2006.

Figure 5

Figure 6: Two shallow slides in the Beylikdüzü district.

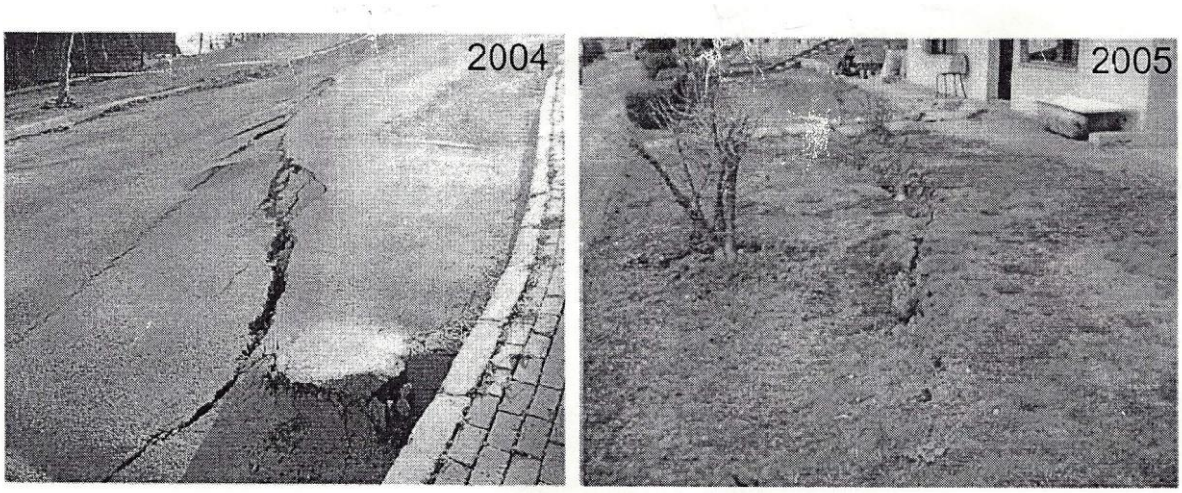

Figure 7**:** Landslide activity and tension cracks on the upper part of the Ambarli landslide in 2004 and 2005.

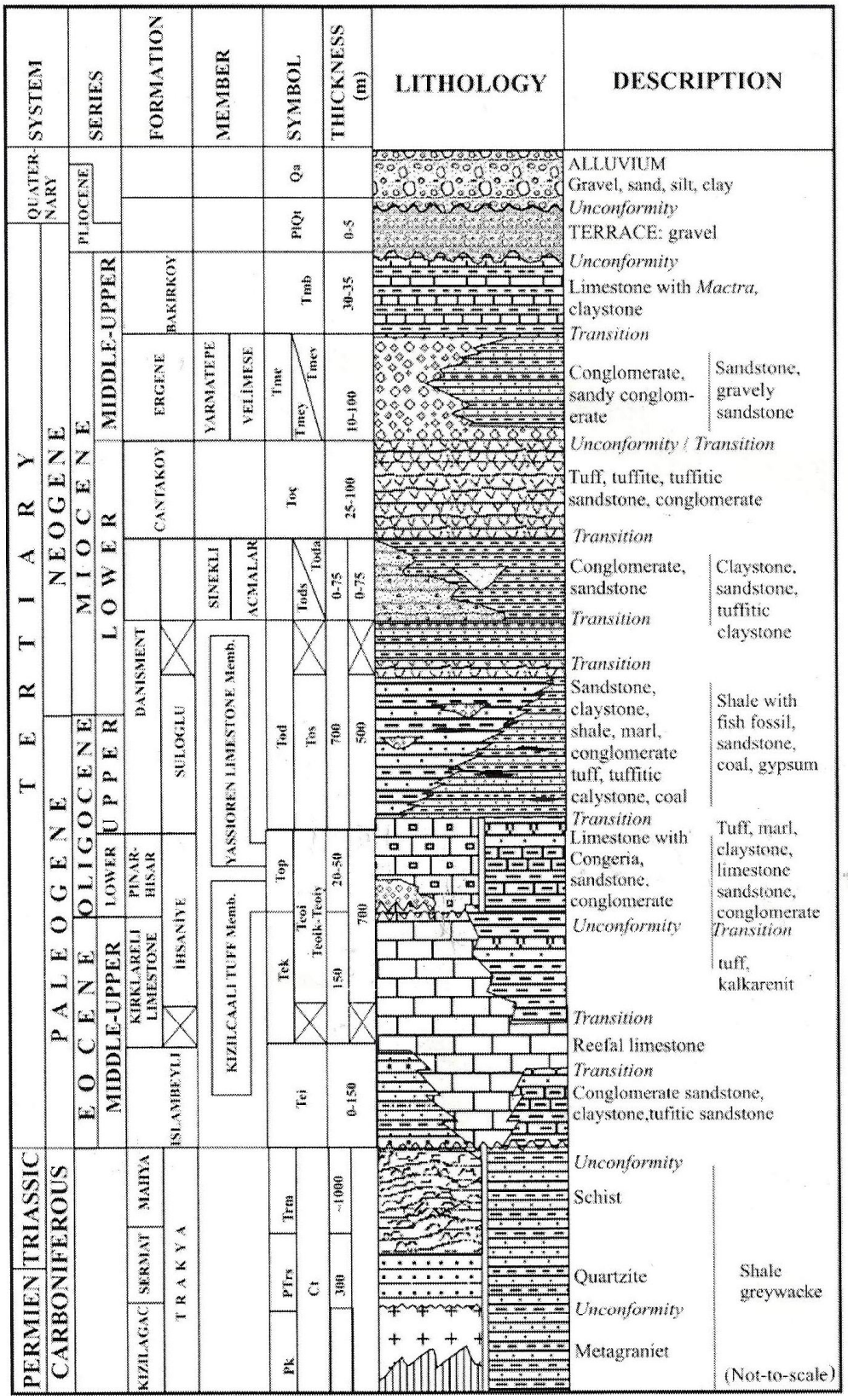

Figure 8: Generalized stratigraphic columnar section of the region (Duman et al. 2004).

2.4 Some References

Arpar E., (1999) Büyükçekmece ile Kûçükçeklece (Istanbul) Heyelenlerinin Genel Özellikleri ve Yrattiklari Baslica Sorunlar: 52. Türk.Jeol.Kurultayi Bildiriler Kitabi, Anakara, 17-23 (in Turkish).

Duman TY, Kecer M, Ates S, Emre O, Gedik I, Karakaya F, Durmaz S, Olgun S, Sahin H, Geomenoglu O (2004) Istanbul metropolü batisindaki (Küçükçekmece – Silivri – Çatalca yöresi) Gekmenoglu O (2004) Istanbul metropolü batisindaki (Küçükçekmece – Silivri – Çatalca yöresi) kentsel gelis, me alanlarinin yerbilim verileri. MTA, Special Publication No : 3, p 249 (in Turkish).

Duman T.; Çan T. Ulusay R., Kecer M, Emre O, Ates S, Gedik I, (2005). A geohazard reconnaissance study based on geoscientific information for development needs of the western region of Istanbul (Turkey). Environ. Geol. DOI 10.1007/s00254-005-0026-y.

Duman TY., Çan T., Gökçeoğlu C., Nefeslioğlu H.A., Sönmez H., (2006) Appolication of logistic regression for landslide susceptibility zoning of Cekmece Area, Istanbul, Turkey. Environmental Geology, 54, 241-256.

Özgül N., (2005) Istabul Il Alanin Genel Özellikileri : Istanbul Büyüksehir Belediyesi Planlama ve imar Daire Baskanliği, 78s. (yayimlanmamis).

Sayar C., (1977) Istanbul Yeni Iskan Yörelero Geoteknik ve Sismik Etüdü : ed. Tezcan, Boğaziçi Ü.Deprem Müh. Arastirma Enst., Cilt 1, 119s (I Turkish).

Yildrim M., and Savaşkan E., (2003). A new approach to statigraphy of tertiary sediments at Istanbul and their engineering properties. In : proceedings of Geology of Itanbul. The Chamber of Geological Engineers Publication, 87-102 (in Turkish with English abstract).

3 DATA RECOVERY AND SHARING

First months of Marsite project were essentially dedicated to the tasks of identifying, recovering, collecting and preparing data for data sharing. Most pre-existing data recovery and sharing work was mainly bore by the Turkish partner, i.e. Tubiak MAM, University of Istanbul and Technical University of Istanbul. A field visit was also organised and mainly referenced publications on field investigations were shared as well.

Recovered data was related to pre-existing GIS with landslide mapping (Duman et al., 2005). A pre-existing dataset has been transferred to the partners by Tubitak, including the high resolution DEM file and the landslides Shape file, also, all made available in the ftp Marsite projet internet area.

Besides this, identification, collection and preparation of data of hyperspectral and multispectral data for the area of interest, of scenes from the HYPERION sensor on board of the EO-1 satellite, Terra-ASTER granules, free sample of multispectral VHR data Digital globe and also some historical data from declassificated CORONA USGS. These data were necessary for processing of the remotely sensed imagery to extract various indexes for the soil and vegetation status and dynamics of urban areas.

During the technical meeting hold in Avril 2013, presentation has been made by Tubitak about the recently launched Istanbul Municipality/Tubitak (so-called IBB project) important geotechnical investigation project in preparation and related to the detailed geotechnical and geotechnical surveys of the belik landslide hazard. This IMT project, called also, included 69 investigations boreholes drilled in 2013 – 2014 aiming to better characterize the landslide hazard. The planned boreholes are 40 m deep up to 200 m, cumulating 4100 m of drilling throughout the westward half-part of the peninsula. Most boreholes are equipped for mobile inclinometer measurements and/or water table measurements. This presentation preceded a field visit of the Avcilar Peninsula focusing on three main spots of main interest, all located in the westward side of the peninsula.

4 SEISMIC LANDSLIDE SUSCEPTIBILITY

4.1 The susceptibility to earthquake-induced on-shore landslide reactivation in the Avcilar-Beylikdüzü peninsula

Susceptibility to seismic-induced landslide reactivation in the Avcilar-Beylikdüzü peninsula is a key issue of the research work undertaken by the partners through Marsite WP6.

A main approach to study this susceptibility to seismically-induced landslide was undertaken essentially by IFSTTAR-La Sapienza, using an unconventional pseudostatic numerical modelling approach, as described in (Delgado et al., 2014).

The nine rototranslational landslides inventoried in the frame of the project (whose length varies from 100 up to 1000 m) are intensely urbanised areas and their extension significantly increased during the last decade. The landslides involve heterogeneous deposits ascribable to Upper Oligocene and to Lower Miocene Formations, which include stiff clays, siltstones, tuffs, sandy-gravels and marls. The slope stability conditions under seismic action were evaluated for a seismic hazard corresponding to a return time of 475-yrs. To this aim several sine-waves characterised by different frequency and phase were considered. To perform the unconventional pseudostatic analysis a distribution of the horizontal pseudostatic coefficient (kx) was applied to each landslide mass for each considered sine wave. As it resulted from this analysis, the slope stability conditions under seismic action, evaluated by the safety factor (SF), significantly change with varying frequency and phase of the sine waves. Critical frequency and phase values can be associated to each landslide mass, indicating the SF sensitivity to these parameters. Susceptibility maps for the existing landslide masses were obtained in terms of SF for a PGA of 0.35g (i.e. corresponding to a 475-yrs return time) and at different slope conditions. According to the obtained results, about 33% of the inventoried landslides have susceptibility higher than 50% to be reactivated by a 475-yrs return time expected earthquake. Based on the computed percentages of susceptibility and considering the urban expansion of the landslide areas during the 2002-2012 decade, it was possible to graduate the relevance of the inventoried landslides for further numerical modelling that will be focused on the local seismic response analysis and on the evaluation of earthquake-induced displacements.

4.2 Landslide inventory and expected actions

The area is of particular interest for landslide susceptibility to earthquake trigger as it is was recently struck by the 17 August 1999 Mw 7.4 Kocaeli and by the 12 November Mw 7.2 Düzce earthquakes. Moreover, several studies showed that the Avcilar area (Figure 9) suffered significant damage (Dalgiç, 2004), largely due to the amplification of the earthquake ground motion. In fact, for this area, an intensity of VII (MSK) was assigned, while in the other districts of the metropolitan area an intensity of VI (MSK) was generally observed (Gruenthal, 1988; Ozmen, 2004). According to Erdik et al. (1999) the expected PGA on soft rock in the Avcilar-Beylikdüzü varies in the range 0.3 – 0.4g for a 475-yrs return time while it ranges from 0.2 up to 0.275g according to Atakan et al. (2002). These PGA values are also in very good agreement with the fault rupture scenarios proposed by Pulido et al. (2004) along the NAF in the Marmara Sea region. The anomalous amplification of the ground motion observed in the Avcilar area is considered to be mainly related to the presence of soft sediments overlaying a stiff seismic bedrock; the fundamental resonance frequency mainly range from 0.1 up to 2 Hz with local values up to 5 Hz (Ergin et al., 2004; Picozzi et al., 2009). In general, the amplified bands are less than 4 Hz, and the physical properties of the geologic materials are capable of amplifying the motions by a factor of 5-10 (Ozel et al., 2002).

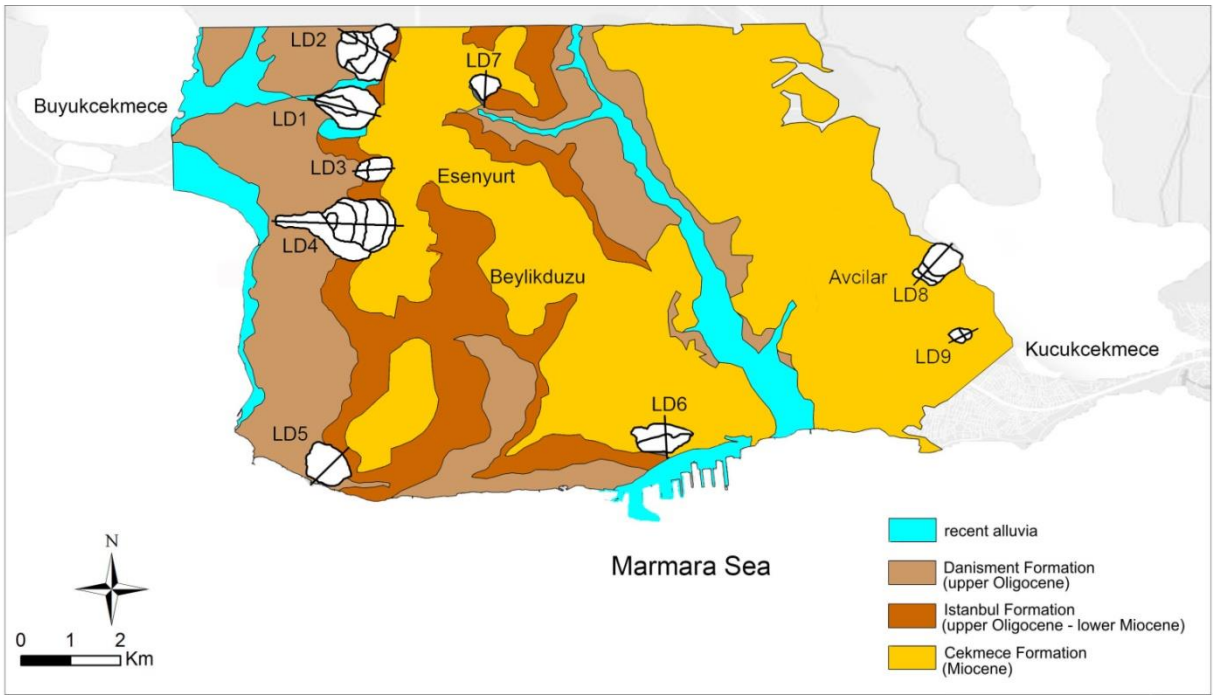

Figure 9 : Study area and inventoried rototranslational landslides

As it results from previous studies, the Avcilar-Beylikdüzü peninsula has a high susceptibility to slope instabilities as almost the 84% of the area is landslide-prone (Duman et al., 2006). About 19% of the area is covered by deep-seated landslides that are primarily located in sandstones with interbedded permeable and impermeable layers such as clay-stone, siltstone and mudstone and about 32% of the total landslide area corresponds to these deposits.

No literature data or technical documentation exist on earthquake-induced reactivation of landslides in the Avcilar-Beylikdüzü peninsula nor due to the recent 1999 Kocaeli and Düzce earthquakes neither to older historical earthquakes; nevertheless, it is not possible to exclude that the strain rate of continuously active landslides increased after the occurrence of earthquakes as well as that sliding movement were induced along shear zones without generating so evident or checked landforms.

For this reason this study is focused on a quantitative evaluation of the slope stability conditions under dynamic shaking for already existing landslide masses that are characterised by main rototranslational mechanisms (Hungr et al., 2014). At this aim, an inventory map was detailed after field surveys; 9 rototranslational landslides were recognised (Figure 9) whose width varies from 250 up to 1000 m and length ranges from 300 up to 1850 m. The maximum depths of the sliding surfaces range from some tens up to 100 m and the rototranslational mechanisms generally show a multiple style (sense of Varnes, 1978), i.e. with visible counterslope terraces and secondary scarps (Figure 12); the landslide volumes vary in the range of 1 up to 100 Mm^3.

Most of the landslides are located along the costal slopes; the largest ones (landslides LD1, LD2 and LD4 of Figure 9) are located in the western portion of the peninsula (in the Büyükçecmece - Beylikdüzü area), where they widely involve buildings and roads, while the remnant landslides are sparsely distributed in the peninsula, along the southern and the eastern coasts (i.e. Marmara Sea and Kucukcekmece Lake respectively).

Based on the geological cross sections specifically obtained along each landslide slope, in the western sector of the Avcilar-Beylikdüzü peninsula, an 100 m thick succession of marls and sand deposits (ascribable to Bakirköy and Kiraç members) that overlay tuffs and clay-stones (ascribable

to the Danisment Formation) are generally involved in the landslides. In the southern sector of the peninsula the landslides involve siltstones, tuffs and silty-clays deposits (ascribable to Cantaköy member and Danisment Formations) overlaid by a layer up to 50 m thick of sandstones and marls (ascribable to the Kiraç and Bakirköy members). In the eastern sector of the peninsula the landslides involve silty-clays, sands and marls (ascribable to the Çekmece Formations).

4.3 Unconventional pseudostatic approach

In order to analyse the slope stability conditions under seismic shaking an unconventional pseudostatic approach (Delgado et al., 2014) was applied in this study. Following such an approach, the restrictions imposed by the conventional pseudostatic analysis can be limited by considering several distributions of the horizontal pseudostatic coefficient kx, and of the related pseudostatic force, that can be obtained by varying the horizontal acceleration values within the landslide mass (kx(x)) according to the sine waveform (Figure 10).

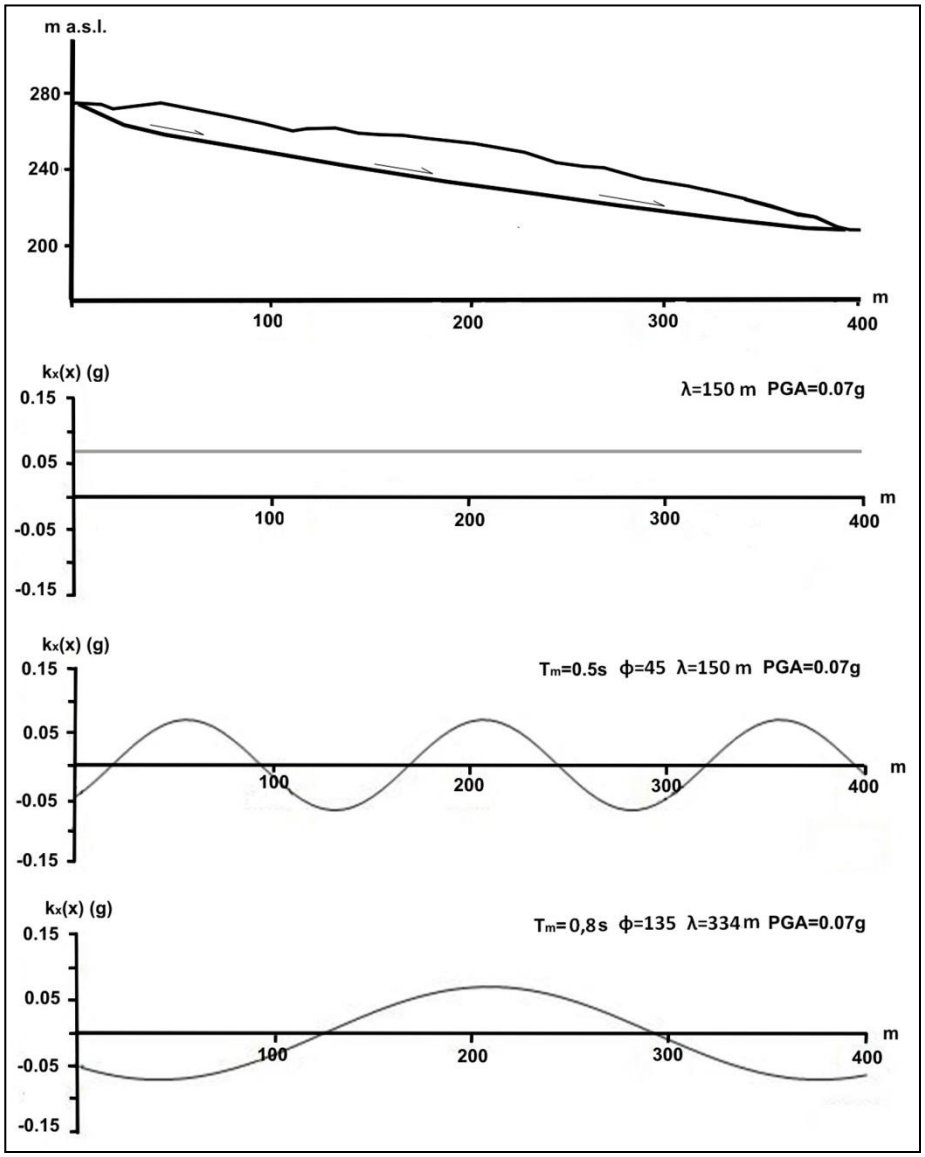

Figure 10 : Sketch illustrating the unconventional pseudostatic approach here adopted for evaluating the landslide stability under seismic action.

Because the seismic wavelength (λ) changes with the value of Tm, the kx(x) distributions are characterized by decreasing spatial variation with increasing Tm (i.e., the half-length of the sine wave becomes equal to the landslide length). For a null frequency (i.e., an infinite seismic wave period), the assumed conditions are theoretically identical to the pseudostatic ones (kx is equal for all the slices considered in the slope stability analysis). Based on the here-applied approach the Safety Factor (SF) value distribution can be reported as a function of the sine wave frequency (fm=1/Tm) only (SF_{fm}) or of both the fm and the Φ values ($SF_{(fm,\Phi)}$). For each (kx(x)) distribution the slope stability conditions of the landslides were evaluated by a limit equilibrium analysis using the simplified method of Bishop (1955) under the assumption of a rigid block model, i.e. by neglecting plastic internal deformations of the landslide mass. At this aim, the mechanical properties of the involved materials were attributed according to literature data (Cetin et al., 2004; Dalgiç, 2004) and were diversified along the sliding surface; the hydraulic forces were accounted for by the pore-pressure parameter r_u (Bishop, 1955).

4.4 RESULTS

4.4.1 Sensitivity analysis

A sensitivity analysis to the seismic wave properties and to the slope conditions was performed in order to obtain the $SF_{(fm\ \Phi)}$ distribution for r_u varying from 0 (i.e. dry conditions) up to the maximum admissible values (which varies from a ratio of 0.3 up to 0.6 depending on the landslide geometry). At this aim, fm values ranging from 0 to 3Hz were considered. To account for the variation of the dynamic properties of the landslide masses, the $SF_{(fm,\ \Phi)}$ distributions were obtained for two values of Vs, 200 and 400 m/s respectively, according to the available data (Cetin et al., 2004; Picozzi et al., 2009). As discussed before, a PGA of 0.35 g was considered in this study as it is representative for an expected earthquake of 475-yrs return time focused along the NAF.

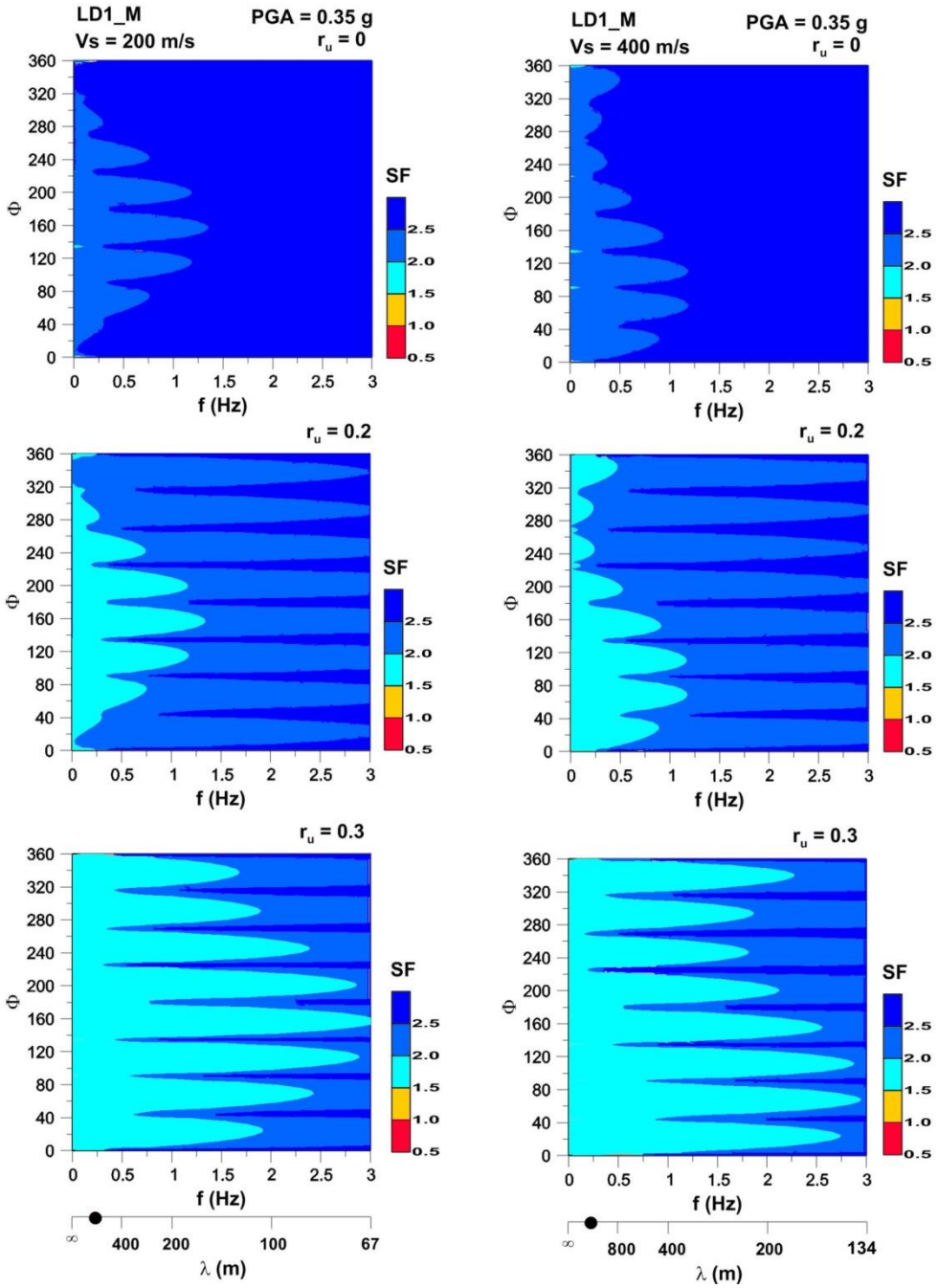

Figure 11: Variation of SF depending on f_m and Φ along with the pore pressure r_u as it results for the landslide LD1 of Fig.11.

To obtain a more detailed analysis of the landslide stability conditions of the landslide slopes, the unconventional pseudostatic analysis was performed not only for the main sliding surface of each landslide but also for the secondary ones. At this aim, each landslide mass was distinguished in a number of sub-masses equal to the main plus the secondary scarps, i.e. corresponding to main and secondary sliding surfaces; each sub-mass was delimited by the respective secondary surface. The so obtained 22 sub-masses of the 9 inventoried landslides were analysed separately according to the Bishop method and to the unconventional pseudostatic approach.

The obtained $SF_{(fm,\ \Phi)}$ distributions demonstrate that the sensitivity to seismic wave properties, i.e. the variation of SF depending on fm and Φ increases with increasing landslide dimensions as exemplifies by the results obtained for landslide 1 (Figure 11).

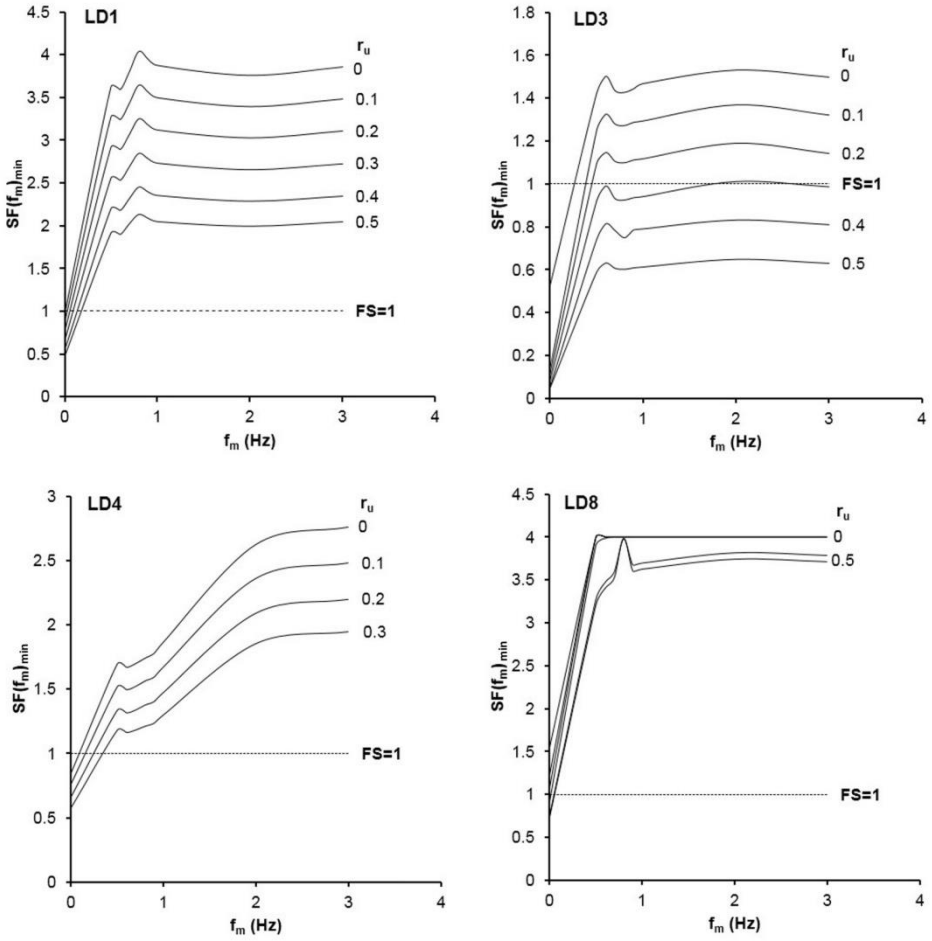

Figure 12 : $SF(f_m)_{min}$ distributions with varying pore pressure r_u obtained for the landslides LD1, LD3, LD4 and LD8 in case of Vs equal to 200 m/s.

An interesting $SF_{(fm)}$ distribution can be obtained for a fixed r_u by considering the minimum SF values $SF(f_m)_{min}$) computed at a certain f_m value for all the considered Φ. Such a distribution highlights the critical frequency value (f_{m_cr}) as it corresponds to the SF invariance for a fixed r_u. Figure 12 exemplifies the SF ($f_m)_{min}$) distributions obtained for the landslide 1, 3, 4 and 8 in case of Vs equal to 200 m/s.

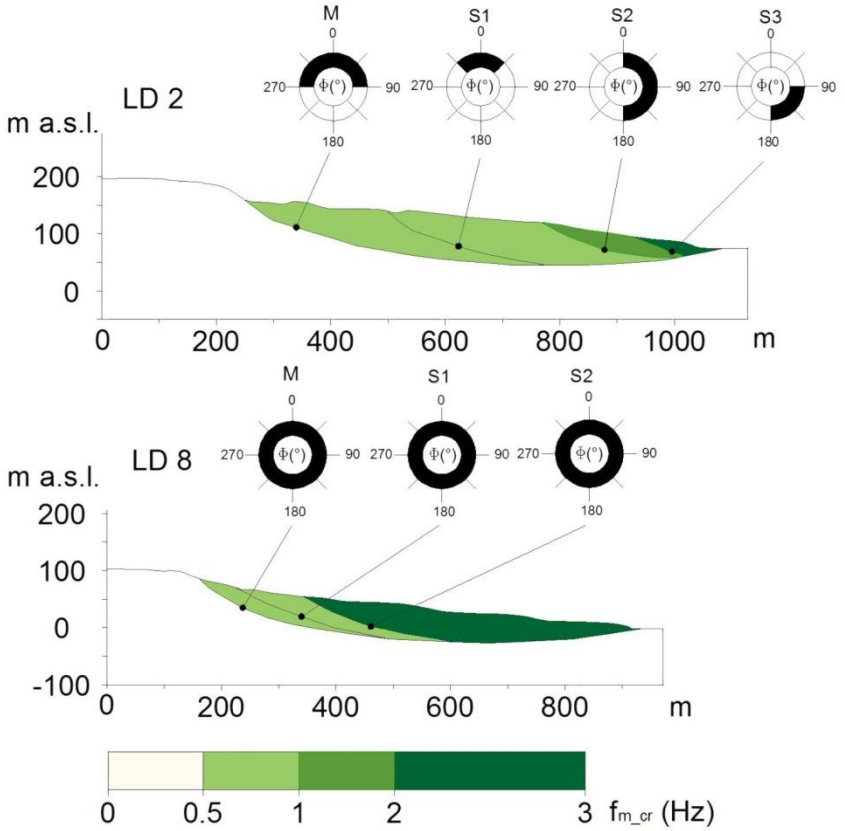

Figure 13 : f_{m_cr} distributions along the landslide mass for landslide LD2 and LD8.

An exemplification of the f_{m_cr} distribution along the landslide mass, i.e. depending on the sliding location as well as of the Φ_{SFvar}, is reported in Figure 13 for landslide 2 and 8, assuming Vs values of 400 and 200 m/s respectively. As it results from these distributions, for the two landslides the f_{m_cr} value decreases moving uphill, i.e. considering longer portions of the landslide mass.

4.4.2 Stability maps

Distribution maps of the f_{m_cr} values were obtained by considering the 22 sub-masses of the inventoried landslides for the two considered Vs values (Figure 14).

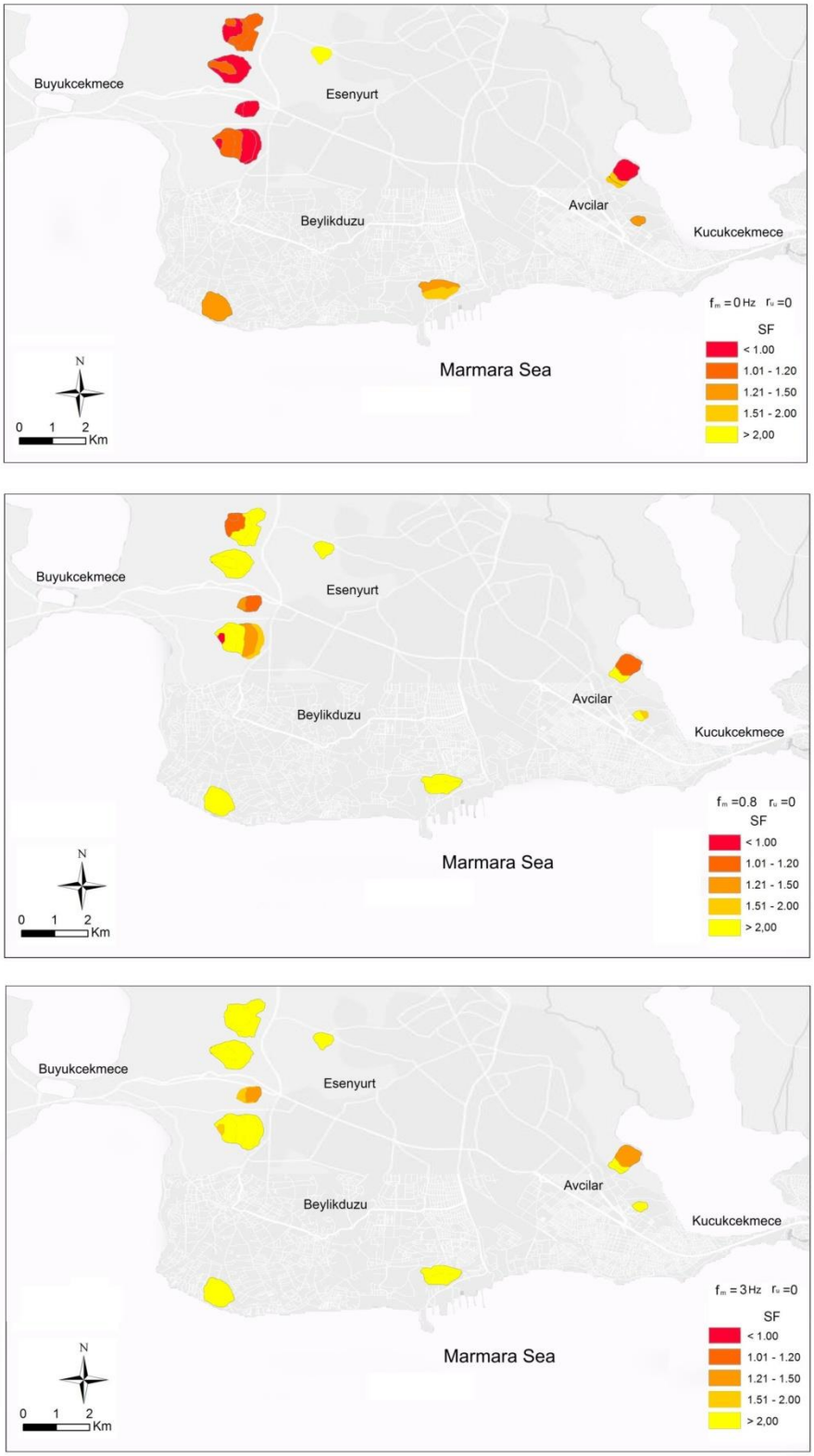

Figure 14 : Example of SF values obtained for the 9 inventoried rototranslational landslides.

As it results from these maps, the f_{m_cr} values generally decrease with decreasing Vs, in agreement with the resulting wavelength within the landslide mass (i.e. wavelength increases with increasing Vs at the same fm and, as a consequence, for a lower Vs, f_{m_cr} corresponds to a lower value).

Similar distribution maps were obtained for the Φ_{SFvar} range in which the SF values depend on fm; nevertheless, such distributions do not highlight a significant relationship nor respect to the landslide mass portioning neither respect to the assumed Vs values.

Based on the above described slope stability analysis, distribution maps of SF values referred to the 22 landslide sub-masses were obtained by considering the different properties of the seismic sine waves (i.e., fm and Φ) as well as by assuming different Vs and r_u values to the landslide slopes. More in particular, Figure 14 exemplifies the results obtained for different f_m and r_u by assuming a Vs equal to 400 m/s and considering the lowest SFs computed among all the possible Φ values.

4.4.3 Susceptibility analysis

In order to quantify the susceptibility to earthquake-induced landslide reactivation, at the here considered seismic hazard (i.e., for an expected earthquake with a 475-yrs return time), a basic probability was computed for each landslide by the ratio between the number of instability occurrences (i.e. with SF<1) and the total considered conditions that are defined on the basis of the f_m, r_u and Vs combinations as exemplified in the distribution maps of Figure 11 and Figure 12 (i.e. considering the lowest SF computed among all the possible Φ values). As each landslide was portioned in sub-masses, an instability occurrence was considered if at least one sub-mass of the landslide itself reached an unstable condition. According to this evaluation, landslides 2, 3 4 and 8 have a susceptibility to earthquake-induced re-activation higher than 40% (Figure 15).

Based on the analysis of the satellite images available on the Google Earth on-line platform for the 2002 – 2012 decade (i.e. after the 1999 Kocaeli and Düzce earthquakes), a Landslide Urbanization Index (LUI) was computed for each inventoried landslide by the percentage ratio between the urbanized landslide area and the total landslide area.

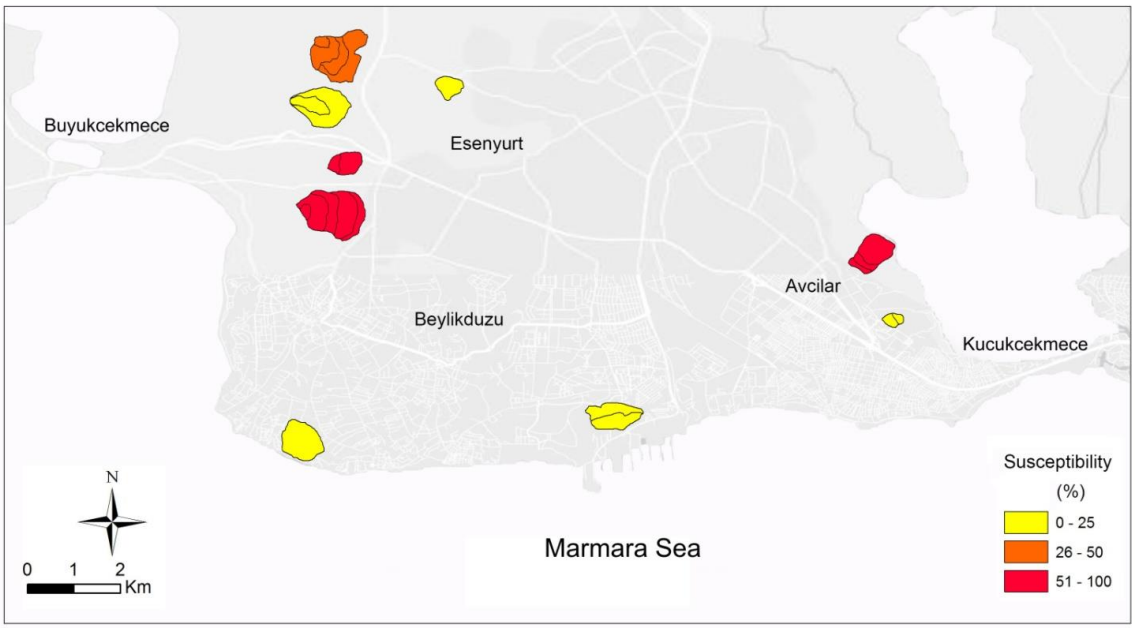

Figure 15 : Susceptibility values for the earthquake-induced landslide re-activation obtained for the 9 inventoried rototranslational landslides.

The LUI values computed for the 2012 satellite view show that only landslides 3, 4, 5, 6 and 7 exceed the 30%; moreover, only in the case of landslides 4 and 7 the LUI increased of almost 500% in the last decade while in all the other cases it remains lower than 50% (Figure 16).

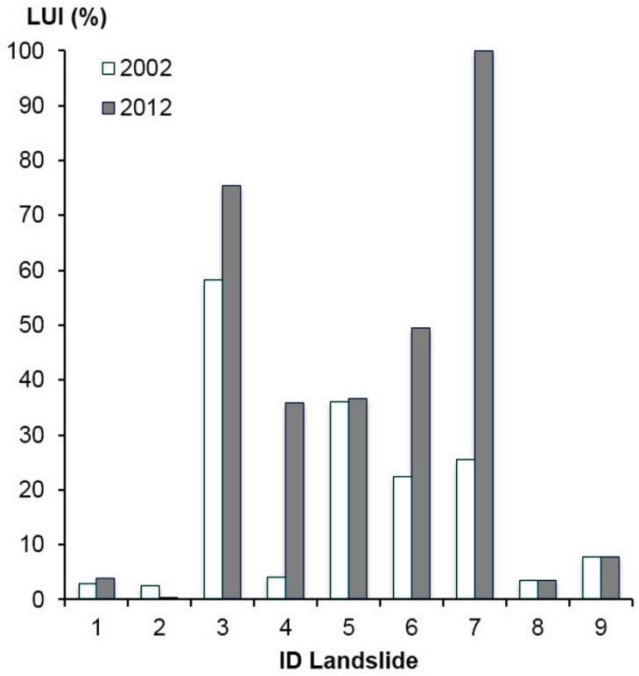

Figure 16 : LUI values computed for the 9 inventoried rototranslational landslides.

4.5 Conclusions

The so-defined LUI is basically a spatial exposition index which helps to graduate the intensity of potential damage caused by landslide re-activation in the urban areas.

Taking into account the percentage of susceptibility and the LUI value computed for each landslide, it results that the highest risk conditions, related to earthquake-induced landslide re-activations, should be expected for the landslides 3 and 4.

Nonetheless, as the LUI increment during the last decade was much more higher in the area of the landslide 4 with respect to the one of the landslide 3, this means that much more novel constructions were realized after the last historical Mw>7.0 earthquakes that occurred in 1999.

For all these reasons it appears of particular interest to carry on more detailed studies and analyses for the landslide 4 (which involves the coastal slope at NE of the Büyükcekmece gulf), focused on the interaction of seismic waves with the landslide mass to quantify the expected earthquake-induced displacements.

5 PHOTOGEOLOGICAL INTERPRETATION

The first aim of INGV's contribution was the integration of geological and geomorphological analyses with high-resolution DInSAR data to allow the identification and characterization of activated and reactivated Deep-seated Gravitational Slope Deformations (DGSD) and, more broadly, generic gravitational phenomena inside the study area.

Firstly, INGV has assembled a GIS with ENVISAT-ERS DInSAR temporal series obtained from WP3 Task3. These temporal series (Figure 17 : map of DInSAR temporal series.

So, to analyze in a deeper manner these results a stereo pair of high resolution (0.6 m) satellite images (Pleiades satellite) was ordered to identify and characterize gravitational phenomena of the study area. These images were acquired within 2 months time period and then a preliminary photogeological interpretation has been carried out.

) evidence some sectors with negative velocities reaching about 25 mm/yr.

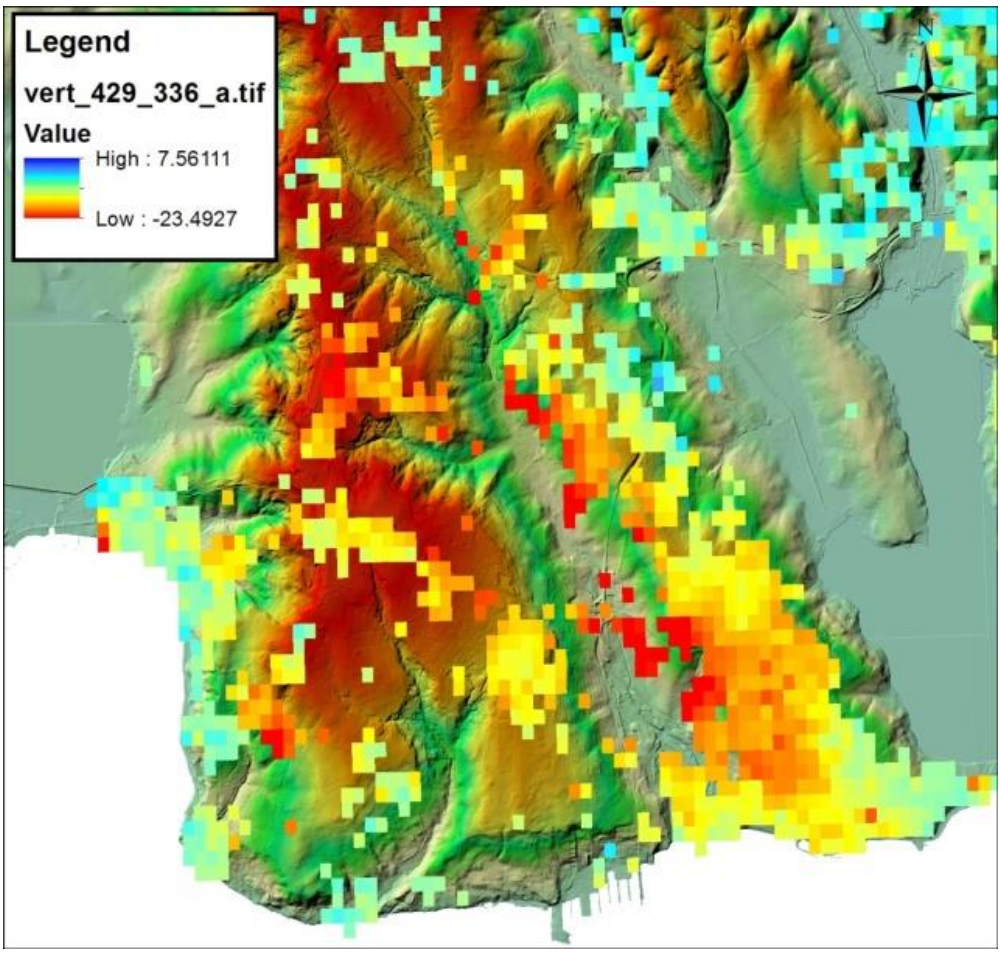

Figure 17 : map of DInSAR temporal series.

So, to analyze in a deeper manner these results a stereo pair of high resolution (0.6 m) satellite images (Pleiades satellite) was ordered to identify and characterize gravitational phenomena of the study area. These images were acquired within 2 months time period and then a preliminary photogeological interpretation has been carried out.

The identified gravitational elements recognized are represented by flows, complex landslides, translations and paleolandslides (Figure 18Figure 18). The above mentioned landslides has been also classified in certain, inferred and quiescent.

Moreover, linear elements associated with landslides as escarpments and paleo-escarpments over a trench associated to a deep-seated gravitational slope deformation were identified. Terraces, paleo-terraces, counterslope terraces, solifluctions and unmapped landslides were also identified.

This preliminary interpretation will be followed by in situ survey and will be compared with ENVISAT-ERS DInSAR temporal series obtained from WP3 Task3.

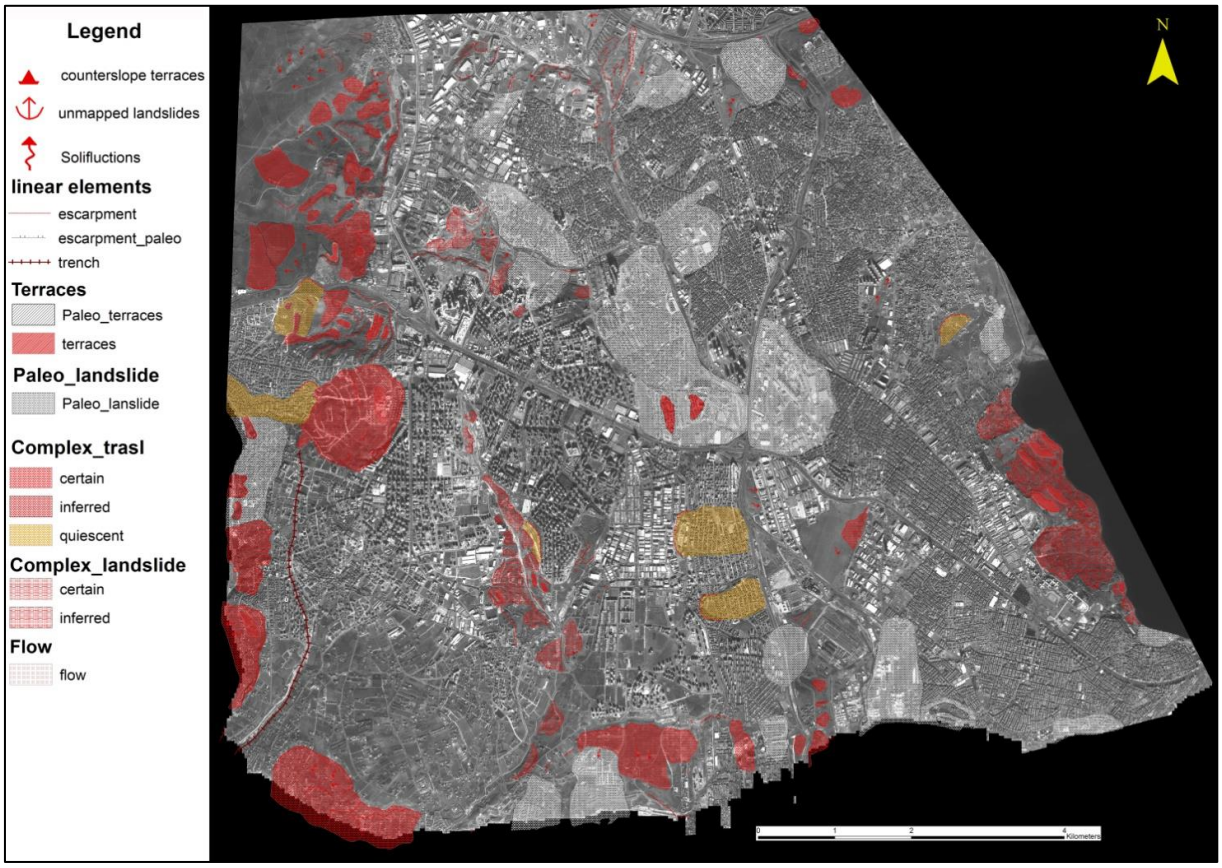

Figure 18 : Results of photogeological interpretation.

6 MULTISPECTRAL / HYPERSTRAL IMAGING

University of Pavia promoted the use of space multispectral/hyperspectral image data to identify geological and geophysical parameters and delineate corresponding areas. This work can be completed to evaluate the resolution and identify landslide hazard-related features.

In order to validate and fulfil these requirements several databases of images, both public and commercial, were explored looking for hyperspectral, multi-spectral and very high resolution (VHR) optical datasets, with the basic idea to develop a cube of multiple and heterogeneous remote sensing data, and in particular hyperspectral data.

The obtained data have been processed to produce and extract parameters about vegetation and land cover conditions (e.g., NDVI, vegetation coverage, impervious soil percentage, ...) to be related with landslide areas (obtained by other databases and new field surveys) and their geomorphological features. This set of parameters is the basis of the work to be done in the next part of the project, that is the detection of positive/negative correlations between these indexes and earthquake induced landslide area. Moreover, these indexes are expected to be relevant in combination with other datasets like Advanced InSAR outputs and data derived from field surveys.

As for hyperspectral data, datasets were found to be much more limited quantitatively than expected, and the availability of space borne hyperspectral data for the area of analysis selected (Figure 19) appeared as really poor. Indeed, less than 10 images were found as regards the Hyperion sensor on board of the EO1 satellite (http://eo1.usgs.gov/).

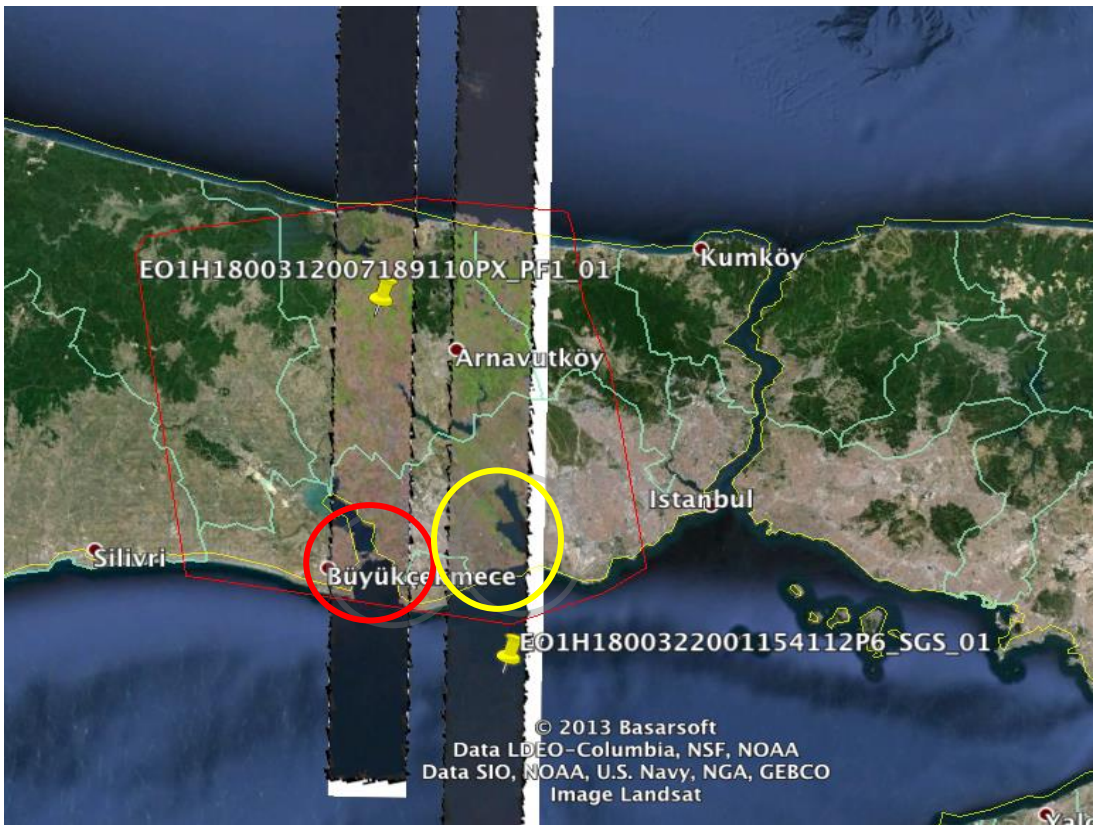

Figure 19: coverage of E01 data for the area of interest.

Nevertheless, these data are still characterized by interesting spectral features because of the hundreds of spectral bands they record in the visible and infrared wavelength ranges (0.4 to 2.4 μm). Unfortunately, their spatial resolution is coarse (30 meters) and the signal to noise ratio is not always satisfactory.

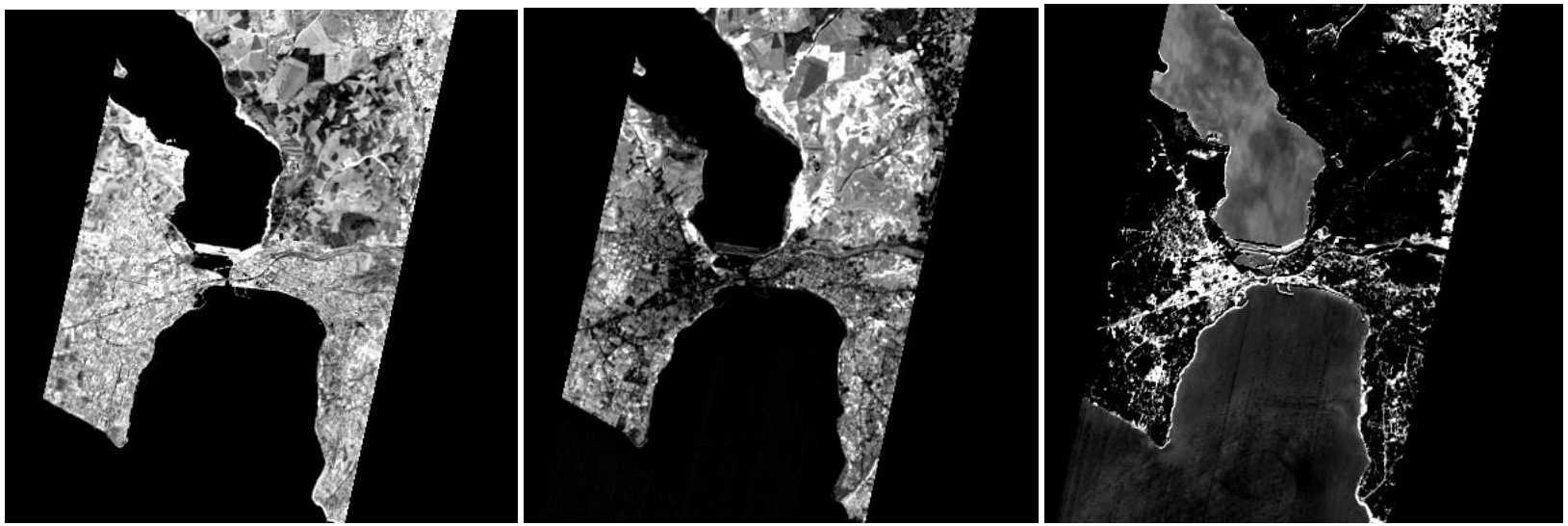

(a) (b) (c)

(d)

Figure 20 : Spectral unmixing results for one EO-1 data set: abundances of (a) rocks (b) vegetation (b) urban, to be compared with (d) a VHR image of the same area, in true colors.

The processing approach applied to the hyperspectral data is called "spectral unmixing" and has been implemented so that we were able to extract percentages of different materials, in turn automatically extracted from the data. Figure 20 shows these results for the area under test, together with their interpretation based on a VHR image of the same area.

Through detailed spatial analysis of the results in Figure 20 and similar ones, a thorough checking was conducted for patterns and relationships between the landslide areas and classification products, including band ratio parameters (e.g., NDVI). Results show clearly that there is not a direct correlation between the imaging derived products and landslides; however the processed data allow to improve the recognition about land use in early 2000's. It is clear that areas affected by landslides are more vegetated than theirs neighbours, and this is related to the higher slopes that reduce strongly the urbanization capabilities.

6.1 Multispectral data image results

Several Landsat images (Landsat 5, 7 and 8) were selected on the area: May 1984, May 1999 (just after Izmit Earthquake), July 2001 and July 2013 and processed to create a Multi-temporal Supervised Automatic Classification of land uses for the area. The output maps are shown in figures 5, 6, 7 and 8 here below.

The results show a notable (and not surprising) increase of the urbanized area, also inside the areas affected by landslides as several field surveys confirm. This fact greatly limits the ability to identify landslides. In addition to this, a number of anthropic deposits or excavations may be confused with landslides or can be affected as landslides.

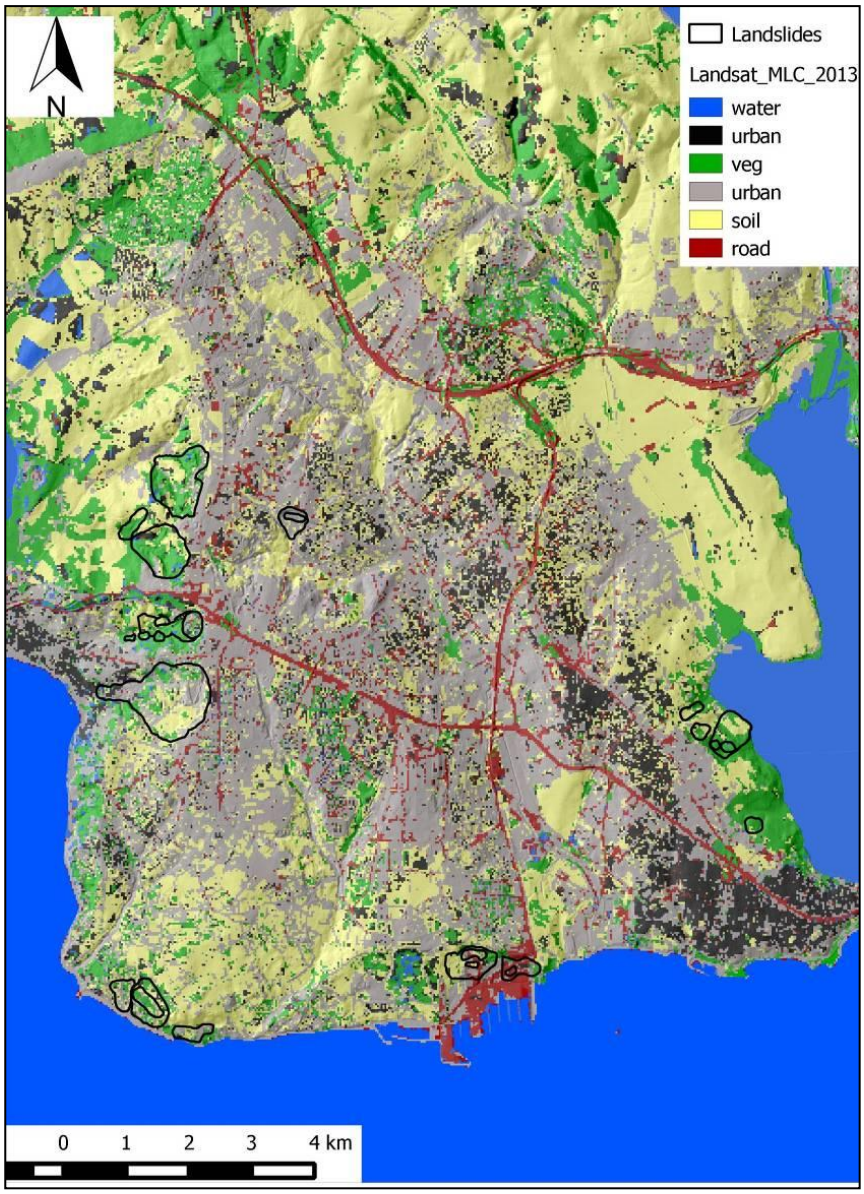

Figure 21 : 2013 Land use map obtained by means of a Maximum Likelihood classifier starting from a Landsat 8 image of July 2013.

.

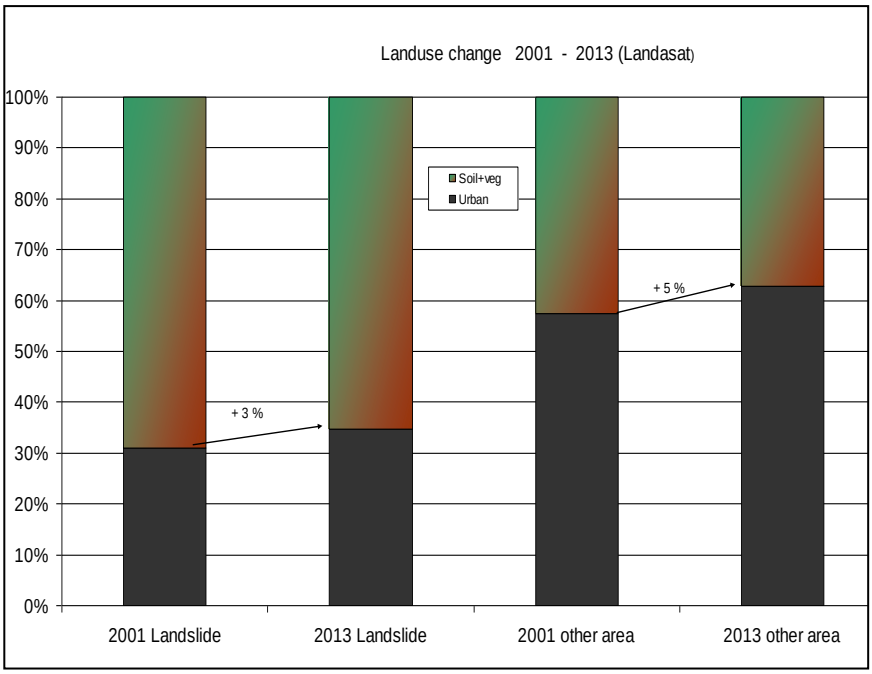

Figure 22 : 2001 - 2013 Urban Areas increase trend.

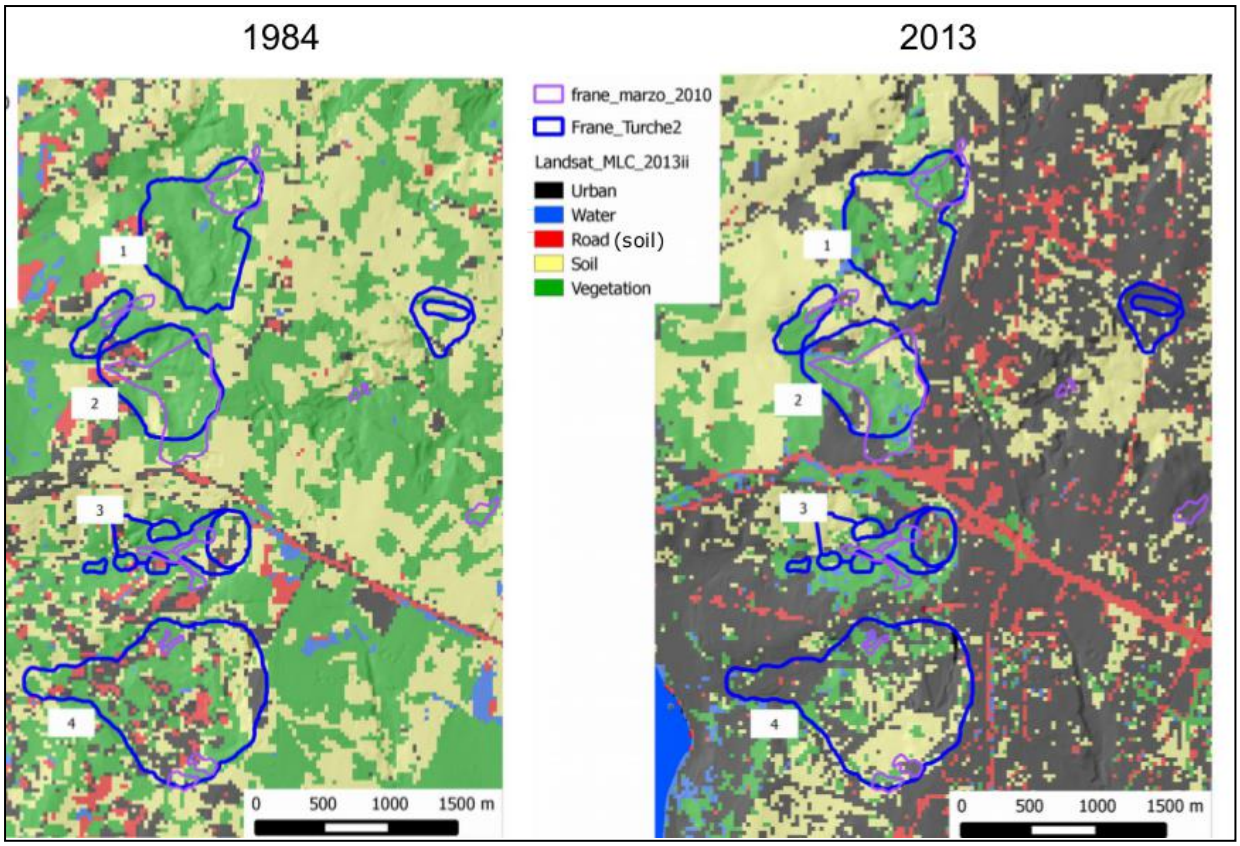

Figure 23 : 1984 - 2013 Land use change (from Landsat data) in east costal area of Avcilar, with a clear highlight of the huge urban growth.

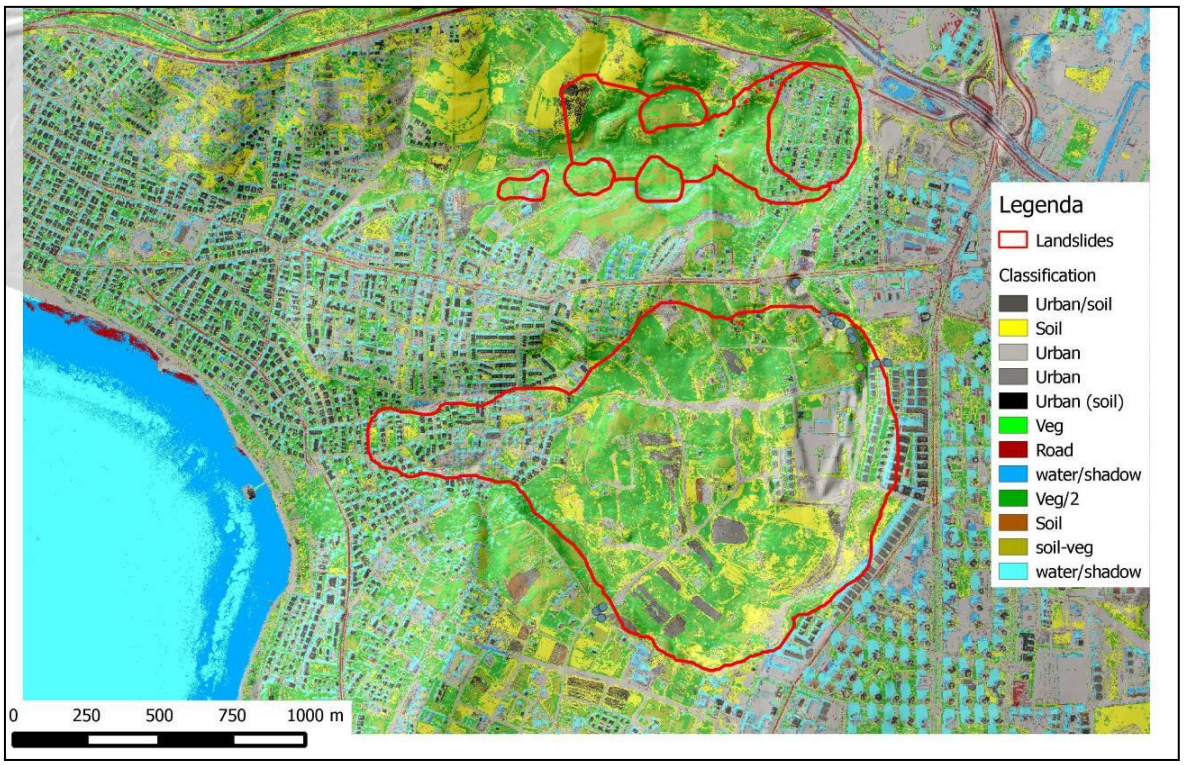

Figure 24 : a detail of the land use map for landslides in the Buyukcekmece area obtained from Landsat (8 July 2013) fused with WorldView II VHR optical data.

6.2 Other dataset analysed

In order to better constrain the onset timing of landslides some non conventional sources were used as follows:

The availability of some aerial photo mosaic from a local map service (http://sehirrehberi.ibb.gov.tr/map.aspx?), about year 1982, allowed to better define some landslide shapes and features. In 1982 the area was strongly less urbanized and the landform was not disturbed by anthropic activity. An interesting consideration can be done: most of the landslides of the area are already present in 1982 and are probably dormant/active. The 1999 Izmit Earthquake probably did not trigger any major landslide in that area, but only reactivate to the most the already existing ones;

Google Earth historical images: from those it is possible to assess landslide activity and the land use change since 2002. From interpretation many landslide consist in shallow earth - slow flows that partially affect some anthropic fills used to plain buildings area (Figure 25). It is more difficult instead to evaluate activity of large and "deep seated deformations". From the same source, combining with meteo data trend from Turkey Meteorological Office was possible to infer that a particular rainy period, in 2009-2010, produces a number of small landslides (shallow slow flow). It is interesting to note from rainfall data since the 1960 to 2012 (Figure 26), that 1981 and 2009-2010 was the rainiest periods of last 50 years (please note that the weather station is quite near).

Some CORONA photos (earthexplorer.usgs.gov) will be processed and analyzed to push at maximum back (1967-1969) the baseline to recognize landslide activities.

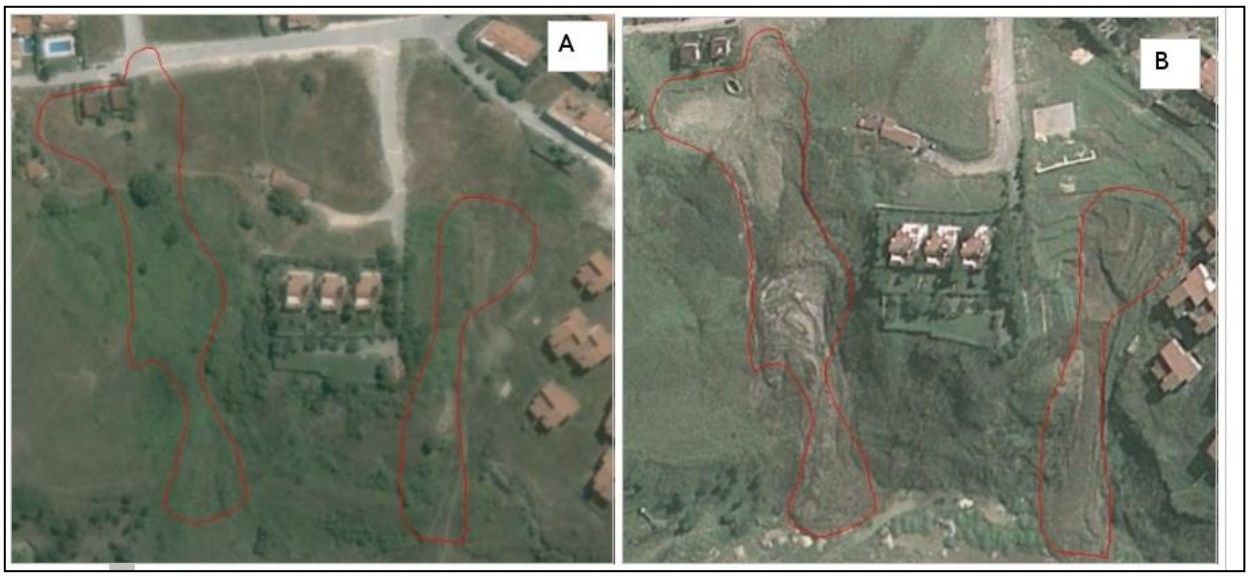

Figure 25 : Active landslide probably dated back to 2009-2010, in the western part of Avcilar peninsula detected on Google Earth Images recorded in 2004 (C -no landslide) and 2010 (B – shallow landslides).

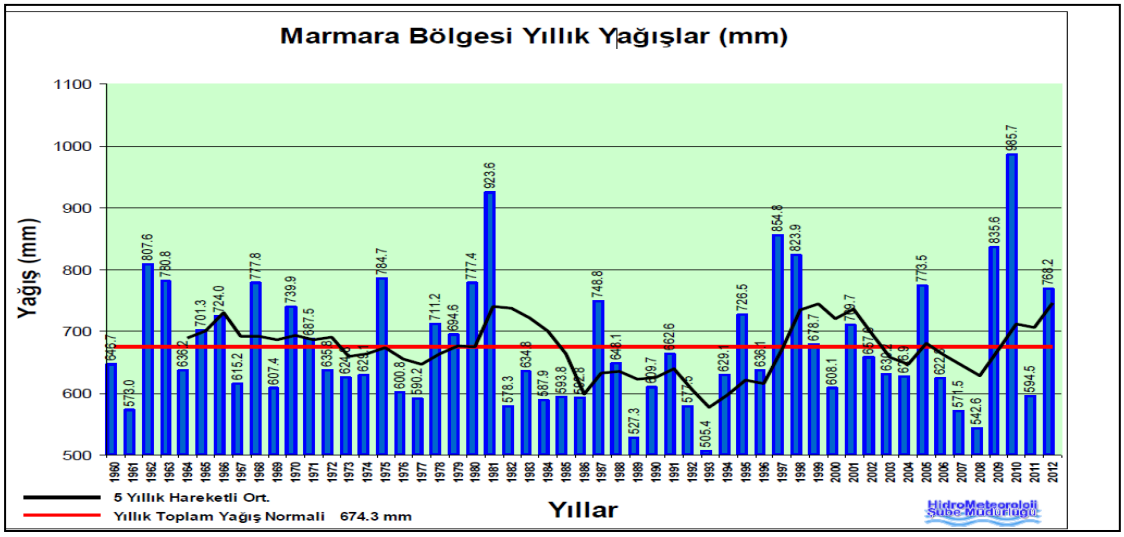

Figure 26 : Marmara area rainfall from 1960 to 2012 by the Turkish Meteorological Office.

6.3 Conclusions

Basically, the primary objective to seek and delineate some positive patterns among geomorphological and land cover/land use features (e.g., parameters like NDVI, impervious soil percentage and related) to derive landslide susceptibility (better an evaluation of ndr) for the area of study, seems to provide a negative result against an unexpected combination of difficulties from the following list:

- Lack of data quality in time and space, in particular hyperspectral data sets;
- Strong heterogeneity of the area under analysis in term of land use/land cover;
- Great dynamics of urbanization, which add disorder-noise in the phase of pattern recognition for the convergence of spectral behavior of derived products (fill and void) with some parts of landslides (e.g., crown and depletion-accumulation area).

7 DYNAMIC MAPPING

In parallel, the tasks described here above, INERIS contribution for the tasks 1.b and 2.b was focused on:

- A methodology to develop a dynamic system to create combined earthquake and rainfall induced landslides hazard maps at near real time and automatically. This innovative system could be used to improve the prevention strategy as well as in disaster management and relief operations (task 1.b).
- The selection of a pilot site to instrument with a multi-parameter observational local network (task 2.b) in order to collect data of interest.

7.1 GIS Tool

Based on literature review a dynamic GIS prototype is used to combine theoretical models, variable on-site data (precipitation, site effects, seismic ground motion), products and results obtained by other WP6 partners contributions.

The method suggested is in progress and all the basics are described here after. The automatic hazard map creation, developed in ArcGIS software (by ESRI), is almost operational. However, the method for the acquiring, processing and uploading the "processed data" server (linked to the GIS) must still be worked on. Incoming data from a field instrumentation of a landslide pilot site is expected to be demonstrated if possible.

7.2 State of art

The application of local landslide models can be very time consuming because detailed information on slope geometry, subsurface conditions and geotechnical characteristics has to be prepared for each slope profile analysed. Since the advent of GIS, scientists increasingly focused on regional scale landslide analyses instead of single slopes.

GIS technologies can provide a powerful tool to model the landslide hazards for their spatial analysis and prediction. This is because the collection, manipulation and analysis of the environmental data on landslide hazard can be accomplished a priori much more efficiently and cost effectively (Carrara and Guzzetti, 1999, Guzzetti et al., 1999) as soon as the data of interest are collected and organized.

GIS modeling is the process of combining databases of different spatial variables using a multi-variable function to obtain an output map of interest. One of the main advantages that GIS offer is the development of hazard occurrence models, permitting evaluation of results and adjusting the input variables with new data. Depending on the function type, GIS models are theoretical, empirical or hybrid. Theoretical models have relationships based on theoretical understanding or physical or chemical principles; empirical models are based on statistical or heuristic relationships; and hybrid models employ semi-empirical relationships, theoretical relationships with empirical functions (Bonham-Carter, 1994).

The use of GIS in landslide hazard began in the late 1970s with simple qualitative models and it had evolved to quantitative models and expert systems (Soeters and van Westen, 1996). Now, almost all landslide susceptibility modelling employ GIS. GIS-based hazard analysis can be applied from local scale to large-scale analysis. However, in landslides inventories, GIS is basically used to store and display data.

Most of the physically-based models that are applied at a local scale make use of the infinite slope model and are therefore only applicable to modelling shallow translational landslides. They can be subdivided in static models that do not include a time component, and dynamic models, which use the output of one time step as input for the next time step.

For dynamic GIS applications taking in account the hydrogeological and seismic factors the state of art remains rather poor.

There are two fundamental reference articles; here we present our differences and what we retain.

First work was proposed by Mahdavifar et al. (2008) and the parameter used to generate seismic landslide hazard map is Newmark's displacement. These authors built a GIS-base system composed by: a map of Arias Intensity (based on attenuation relationships) and a map for seismic landslide hazard zonation (based on simplified Newmark's displacement method) in a short time after an earthquake. Generation of such maps is fully automatic. The platform was calibrated using data from the 1990 Manjil earthquake. When a potential damaging earthquake occurs, the server activates the program and sends earthquake magnitude and epicentral location. The program selects the units of database which are located in earthquake prone area. In the next step, the probable fault of the earthquake is determined, and using Arias intensity attenuation relationship, the Arias intensity coverage is generated for the affected area. To determine source to site distance, the nearest horizontal distance between the center of polygons and the fault trace is calculated. If there is not any active fault near the earthquake epicenter, the epicentral distance is used as source to site distance. By joining the Arias intensity and critical acceleration coverages, the Newmark's displacement (Newmark, 1965) converge is created. After completing the analyses, Arias intensity and Newmark's displacement were arbitrarily categorized into ranges. In the last step, the program sends intensity map and seismic landslide hazard maps, as shape format to server for locating in the web.

In this study there are many simplification assumptions for regional assessment of Newmark's displacement, but it should be noted that this parameter do not necessarily correspond directly to measurable slope movements in the field; rather modeled displacement provide an index to correlate with field performance (Jibson et al., 1998). Moreover, the main limitations are variability in nature of shear strength, the type of mapped landslides, etc).

The second work was proposed by Kanya et al., 2011 and the aim was to establish a GIS-based methodology to couple landslide model to shake maps in order to produce real-time slide maps. The necessary data are: digital elevation model, geology, geotechnical parameters and shake maps.

The two main steps in this case are: the implementation of landslide prediction model in ArcGis (calculation of safety factor and yield acceleration of the soil), and the calculation of soil displacement with California Method (Blake et al., 2002) to obtain the ArcGis displacement map. This method was applied at the Campania region (Italy), which is selected based on the availability of soil shear strength parameters and the proximity to the 1980 Irpina (Mw = 6.9) Earthquake. The Slidemap is created to give "near-real-time" information about landslide occurrences in a large area affected by an earthquake.

7.3 Theory of the GIS implemented method for calculating co-seismic landslide displacements

Among the deterministic methods, generally, the determination of theoretical co-seismic displacement is based on Newmark's displacement method. Rigid sliding block analysis is commonly adopted to predict the potential for earthquake-induced landslides. These predictions give the expected level of displacement as a function of the characteristics of the natural slopes and the characteristics of earthquake shaking.

Despite the development of computer programs to conduct rigorous Newmark analyses, it is not always possible to use this method. As an alternative, the Jibson's method, based on the analysis of strong motion records and many regression equations proposed to estimate Newmark's displacement as a function of seismic parameters, was used.

Newmark's method is fully applicable to the area of study yet only a limited set of records are available, making impossible the deduction of a representative regression equation. Therefore, the

Jibson equations (Jibson, 2007), supposed worldwide representative, will be implemented in the GIS (Figure 27).

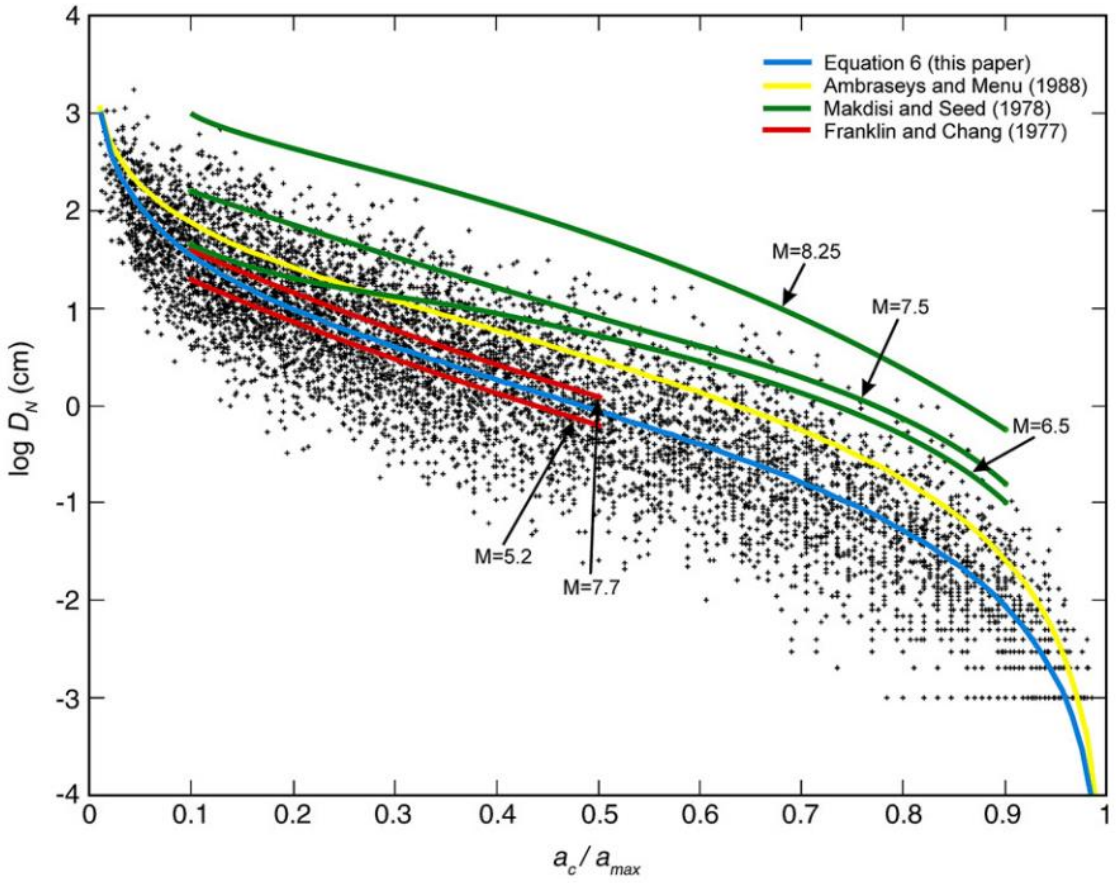

Figure 27 : Examples of regression formulas (coloured) faced to rigorous Newmark displacement (black dots) calculated from the strong motion records (Jibson, 2007).

7.3.1 Implementation of the method in ArcGIS

In order to create a fully automatic hazard map creation, the ArcGIS ModelBuilder application is used as it fits the automation problematic perfectly. As a matter of fact, this application enables to create workflows that string together sequences of geoprocessing tools, feeding the output of one tool into another tool as input. In consequence, what one creates step by step by running manually one process after the other, the ModelBuilder runs it all at once by following the workflow (of the same steps) implemented.

Moreover, it is possible to create and share a model as an ArcGIS tool. Finally, it also enables to integrate ArcGIS with other applications which is convenient for our automatic system which works on a wider dimension that the GIS itself.

The figure below illustrates the model based on the theory described before and currently implemented in ArcGIS.

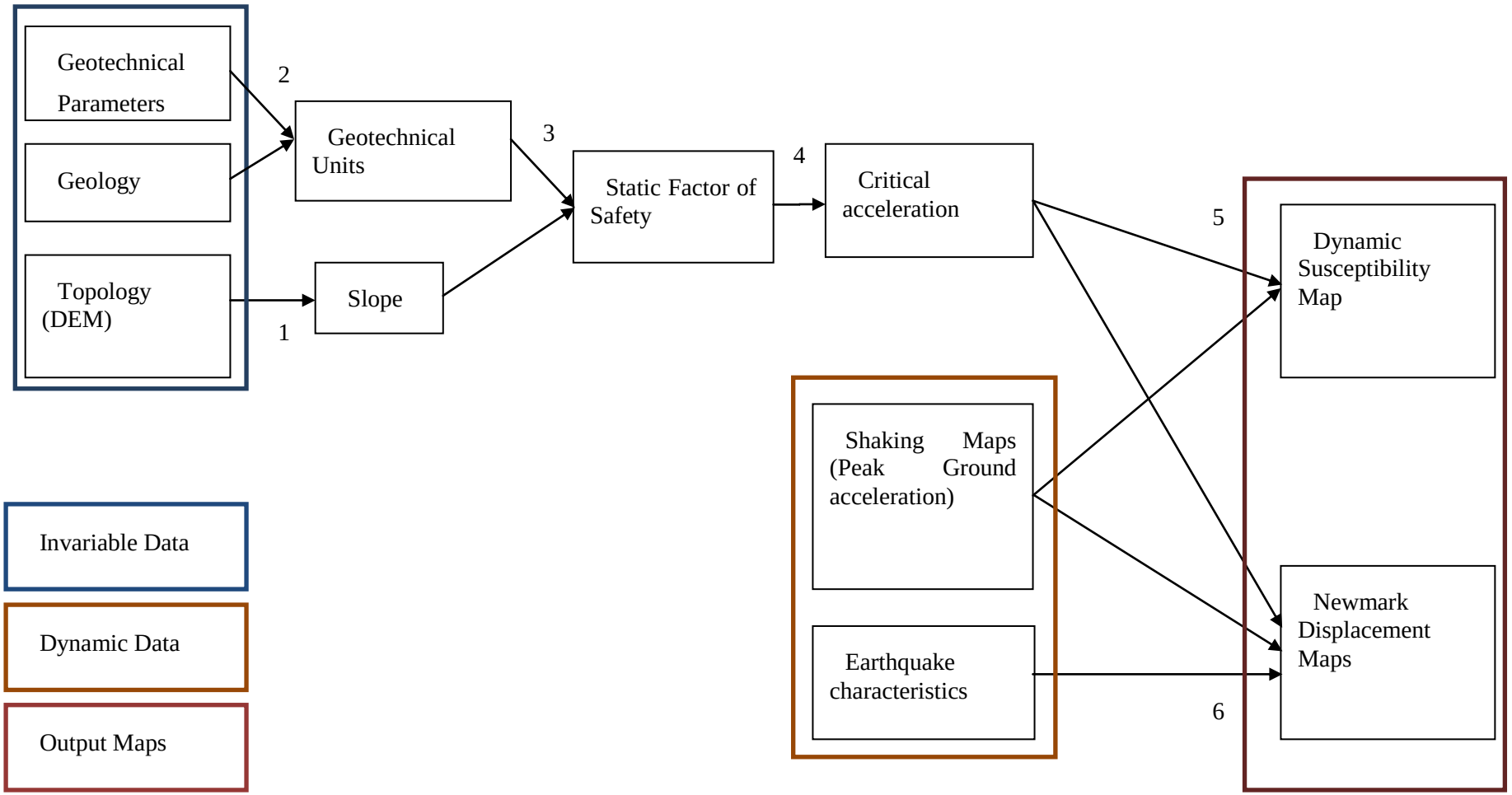

Figure 28 : Chart of the model implemented in the Arcgis Tool at the moment.

The blue and orange squared data in the Figure 28 are the **input data** of the model. They can be split in two main categories:

Invariable Data: The geology and the topology do not change in time and are invariables parameters in the model and are therefore stored in the geodatabase (they can however be updated manually in the active geodatabase if needed).

Dynamical Data: The seismic information (shaking maps, ground motion parameters, etc) are variable parameters in time. This data comes from an external server where the data can be updated externally. The path to this server is given in the model. This enables the model to automatically take in account the near real time updates of the event. It is very important that the nature, format and coordinates of the external information correspond to those expected as input for the model.

Regarding the invariable data:

Geotechnical parameters: is a table file. It gives the geotechnical characteristics of the geological formation. The table is composed of the formation, the cohesion, the friction, the density, the landslide thickness, and the water table thickness above the sliding surface. This table was filled arbitrary as no geotechnical data is yet known. It is expected that this type of information should be provided from the IBB project.

Geology: is a shapefile of polygons. Each polygon represents a geology unit. The attribute table is composed of the objected, the shape nature, the name, symbol and description of the formation. The geological information comes from literature.

Topology: is a raster file (DEM).

As to dynamic data:

Shaking maps: is a shapefile of polygons. Each polygon delimits an area with the same Peak Ground Acceleration. The attribute table includes the value of acceleration (mg). At this work step this file was artificially created in the aim of constructing the automatic GIS structure. The file should be provided by WP9. The model will then have to be adapted to its format.

Earthquake characteristics: is a table file. It gives the earthquake characteristics. The table contains the X position, the Y position, the depth (the hypocenter coordinates) and the magnitude. This file was artificially constructed to integrate parameters needed for the calculation of the co-seismic displacement. The possibility of acquiring such information on a real time scale must yet be discussed with the WP9.

Finally, concerning the all ArcGIS environment, it was based on the topology raster files obtained during the first stage of the MARsite project and caracterized by:

Projected Coordinate System is ED_1950_TM30 and Geographic Coordinate System is GCS_European_1950;

Pixel Resolution (for the raster files) is 5 m².

1. Geo-processes in ArcGIS
2. The succession of geoprocesses, entered as a workflow in the ModelBuilder application, is described below (Figure 29). The numbering of the steps are those of Figure 28.
3. The slope angle raster is calculated (“slope” tool) from the topology.
4. The Geology is joined to the “geotechnical parameters”. Thus, each geology unit has geotechnical characteristics (to do this operation, both files have to be opened).These 2 steps can be run together.
5. The geotechnical parameters for each geological unit are rasterised (“polygon to raster” tool). Thus, cohesion, as well as all other parameters, is given for each pixel of the study area. This operation is necessary to carry out operations between raster maps. For each pixel, the factor of safety is obtained by applying to the slope raster and the geotechnical parameter rasters

this equation: $Fs = \frac{c' + (\gamma - m\gamma_w) Z cos^2 \alpha tan\varphi}{\gamma Z sin\alpha cos\alpha}$ with γ the earth bulk weight in kN/m^3, γ_w the water bulk weight in kN/m^3 , c' the cohesion in kPa, φ the friction angle in degrees, α the slope angle in degrees, Z the depth of the failure surface in meters and Zw the thickness of water above the failure surface in meters.

6. For each pixel, the critical acceleration is calculated ("raster calculator" tool) by applying to the static factor of safety raster this equation: $ac = (Fs - 1) g\ sin\alpha$ with Fs the static factor of safety, α the slope angle and g the gravity of Earth in m^2/s.
7. The Dynamic susceptibility map is calculated from the critical acceleration raster and the real time PGA raster (read from the "processed data" folder described in the first chapter) by subtracting the values for each pixel ("raster calculator" tool).
8. The Newmark's displacement maps are calculated by applying the regression equations (Jibson, 2007) to the critical acceleration raster and the real time PGA raster (read from the "processed data" folder) and taking for Arias Intensity and magnitude the values from the earthquake parameters (also read from the "processed data" folder).

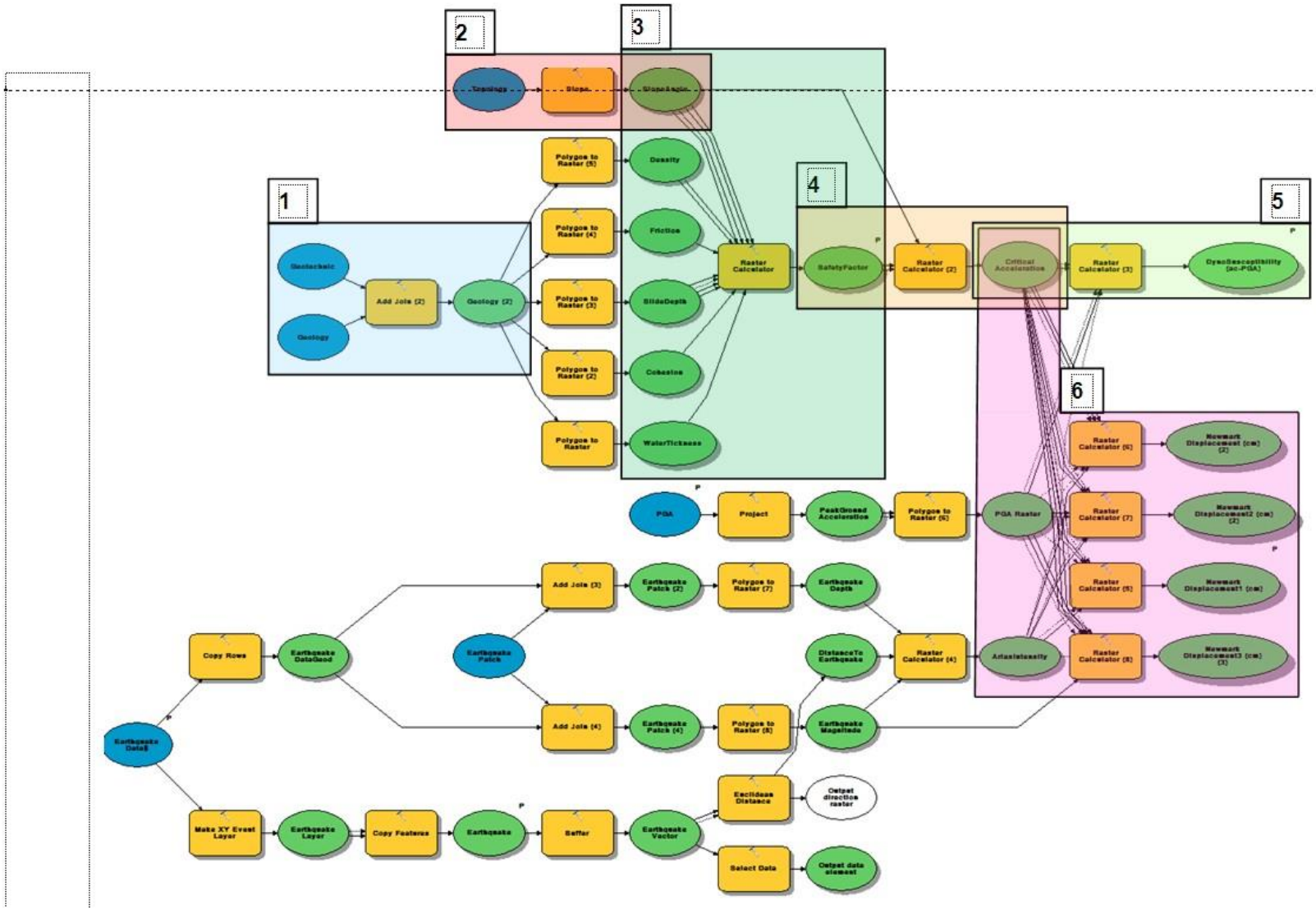

Figure 29: Model chart under ModelBuilder. The numbering corresponds to Figure 28.

7.3.2 Output maps

The output maps obtainded are described below:

1. Dynamic landslide susceptibility map (Figure 30): It simply gives for each pixel the difference between the critical acceleration and the peak ground acceleration. Therefore, it only gives an indication on the areas where a landslide is more susceptible to occur. It does not indicate the extent of the landslide.
2. Co-seismic displacement maps: Figure 31 shows an example of one co-seismic map.

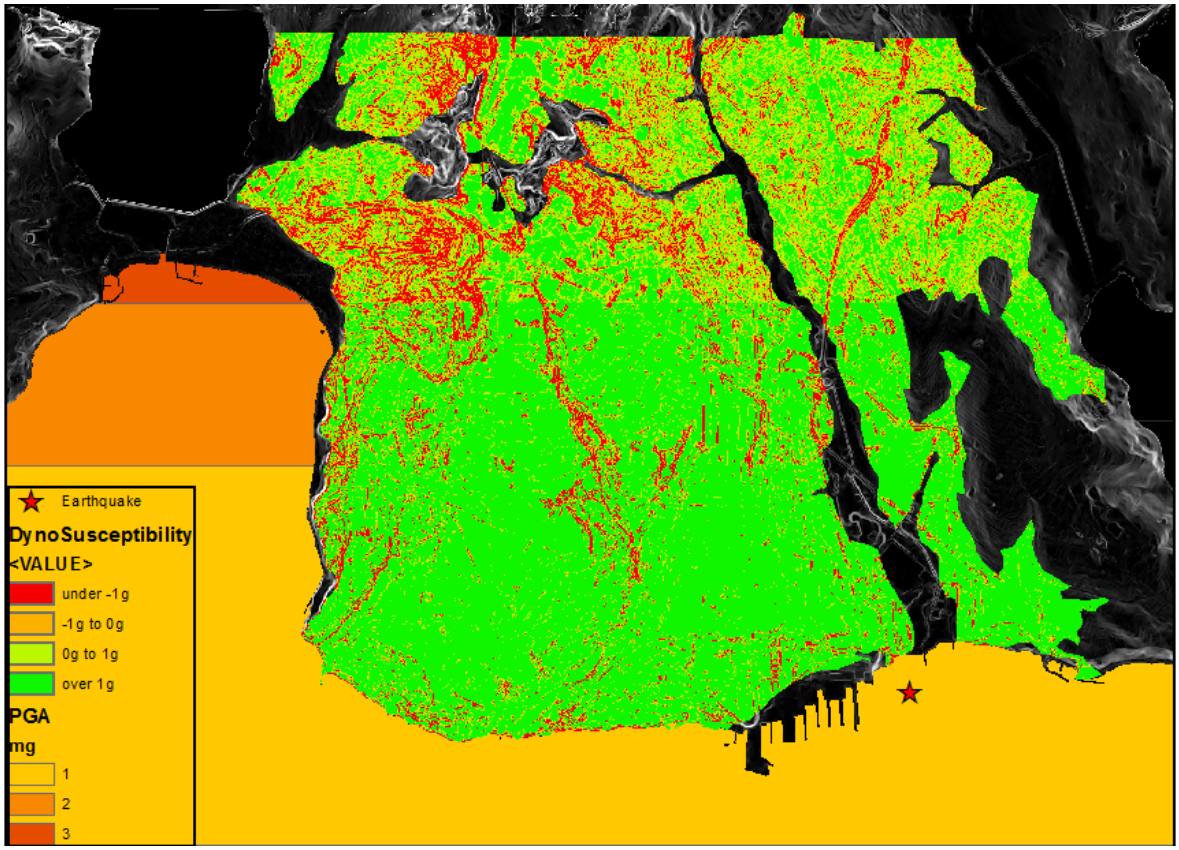

Figure 30 : Dynamic landslide susceptibility map.

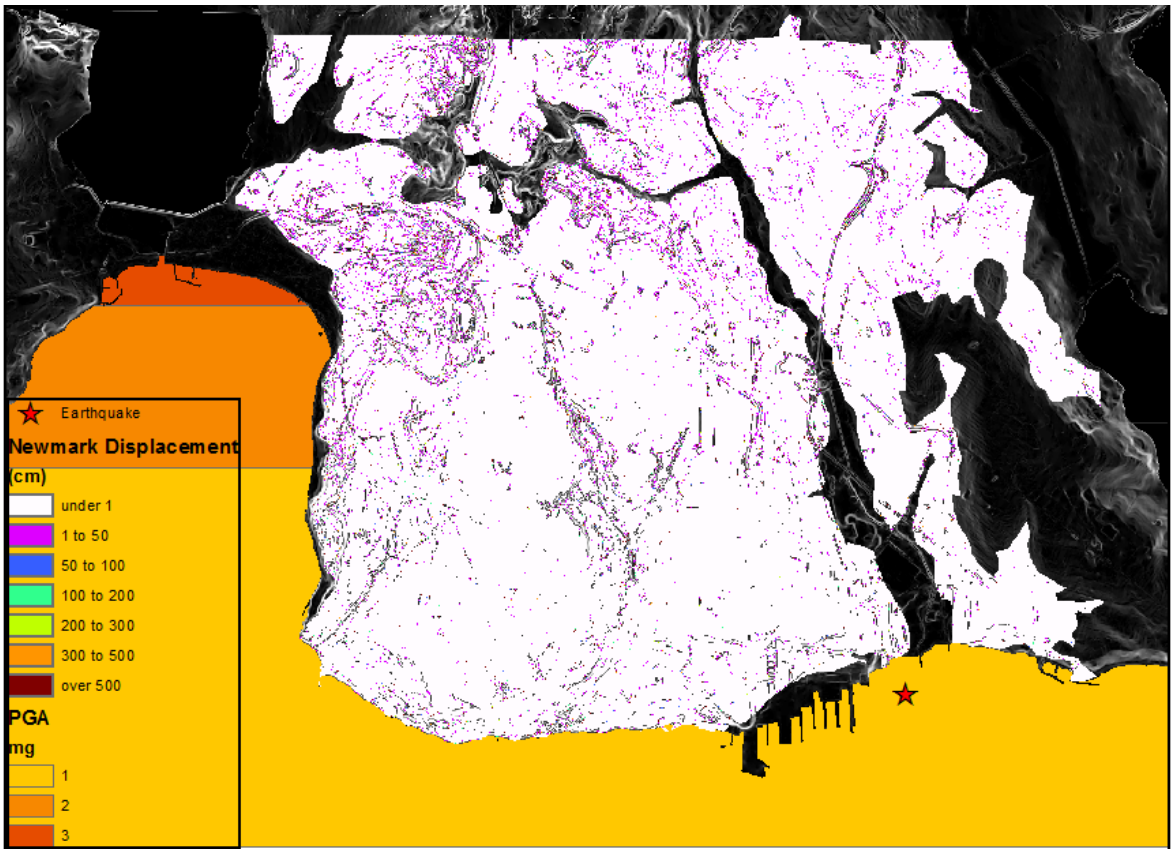

Figure 31 : Newmark's displacement (Jibson, 2007).

It is noted that all parameters have been chosen completely arbitrarily for the moment in the aim to make sure the ModelBuilder works. Therefore nothing can be deducted from those maps else than its appearance.

7.4 Conclusions

This model has a number of limitations. Yet, some improvements of the GIS model and more generally of the automatable system can be made. The limitations are given below, and, when possible, the improvements suggested:

Unknown geotechnical data: Currently, arbitrary values are given to the geotechnical units and therefore false hazard maps. The IBB borehole campaign could give us a representative set of values.

Formula calibration: The formulas obtained (in Jibson, 2007) are calibrated on a wide set of international landslides, for different strong motion types and different ground types. They are therefore maybe not well calibrated for our specific study area. It would be interesting to analyze how the Anatolian strong motions are situated in the regression graph (Figure 27) face to the other records and the empiric formulas. The software SLAMMER developed by the USGS calculates Newmark's displacements by different methods (rigorous and empirical) will enable this analysis. As a matter of fact, it also, contains the records used for the calculation of the empirical formulas. Moreover, they include the records of many seismic stations for the earthquakes of Duzce, 1999 and Kocaeli, 1999. Records can be uploaded in the software. However, if other strong motion records exist for the study area or even for Anatolian fault events, the analysis would be even more precise.

Rainfall integration: No consequent work has been done for the moment in the integration of rainfall in the GIS. The influence of rain on landslides is actually due to the water table level which reduces the soil strength (except earth flows). For the moment the water table level is given and depends of the geology unit. It is planned to link that water table level to the real time quantity of rain.

Nature of landslides: according to the literature, different types of landslides exist in the area (deep, shallow; fall, translational, rotational, flow; new, remobilized by the earthquake). The model currently implemented only takes in account shallow translational new landsides triggered by the earthquake. It would be interesting to consider rotational landslides (bishop's method), remobilized landslides (residual strength on identified sliding surfaces), flows, rock fall triggered by earthquakes.

2D-3D model: The model takes in account only one geological layer per pixel, meaning the landslide occurs only through one geology layer. This is a valid hypothesis for shallow landslides. Yet, if deep landslides have to be simulated, a multiple layering would have to be implemented. 3D GIS methodology would maybe enable a simpler implementation.

Realizing a whole automatic system: only the automatic structure of the GIS is created for the moment by simulating the external sharing folders by independent folders on the computer. A consistent work still needs to be done in the real creation of an automatic global system at the moment only theoretical. In that order, two aspects are to be developed. The first is a thorough discussion and agreement between partners on the localization of the sharing folders, the nature and format of the input and output data. The second aspect to be studied is the method of acquiring in-situ measures and of processing them near real time and to a format implementable in the GIS (one of the aims of the INERIS installation of the pilot site). It is noted that an important informatics programming is to be done to make the whole system automatic (automatic launching of programs, automatic date of launches, etc.).

Further information integration: Much more information can be implemented in the model such as topology update after event, post-event comparison of real displacements (Lidar data) and Newmark's displacements. A thorough discussion with the Marsite WP6 partners will certainly put forward very interesting ideas and the possibility and conditions of realization.

8 References

Atakan, K., Ojeda A, Meghraoui M, Barka AA, Erdik M, Bodare A (2002). Seismic Hazard in Istanbul following the 17 August 1999 Izmit and 12 November 1999 Düzce Earthquakes. Bulletin of the Seismological Society of America, 92(1): 466–482.

Bishop, A.W. (1955). The use of the slip circle in the stability analysis of slopes. Géotechnique 5(1):7–17.

Blake T., H. R. (2002). Recommended procedures for implementation of DMG Special Publication 117 guidelines for analyzing and mitigating landslide hazards in California. *ASCE Los Angeles Section Geotechnical Group* .

Bonham-Carter, G. (1994). Geografic Information Systems for Geoscientists: modelling with GIS. *Elsevier Science* , 398.

Carrara A., G. F. (1999). Techniques and Tools for Mapping Natural Hazards and Risk Impact on the Developed Environment. *Natural Hazards* , Vol. 20: 2-3,93-324.

Cetin K.O., Isik N., Unutmaz B. (2004). Seismically induced landslide at Degirmendere Nose, Izmit Bay during Kocaeli (Izmit)-Turkey earthquake. Soil Dynamics and Earthquake Engineering, 24, 189-197.

Dalgiç S. (2004). Factors affecting the greater damage in the Avcılar area of Istanbul during the 17 August 1999 Izmit earthquake. Bull Eng Geol Env, 63:221–232.

Delgado J., Garrido J., Lenti L., Lopez-Casado C., Martino S., Sierra F.J. (2014). Unconventional pseudostatic stability analysis of the Diezma landslide (Granada, Spain) based on a high-resolution engineering-geological model. Engineering Geology, 184, 81-95.

Duman T.Y., C. T. (2005 (a)). A geohazard reconnaissance study based on geoscientific information for development needs of the western region of Istanbul (Turkey). *Environ Geol 48* , 871–888.

Duman T.Y., Can T., Gokceoglu C., Nefeslioglu H.A., Sonmez H. (2006). Application of logistic regression for landslide susceptibility zoning of Cekmece Area, Istanbul, Turkey. Environ Geol 51: 241–256. DOI 10.1007/s00254-006-0322-1.

Erdik M., Biro Y.A., Onur T., Sesetyan K., Birgoren G. (1999). Assessment of earthquake hazard in Turkey and neighboring regions. Annali di Geofisica, 42: 1125-1138.

Ergin M., Özalaybeya S., Aktara M., Yalçinc M.N. (2004). Site amplification at Aviclar, Istanbul. Tectonophysics 391: 335-346.

Gruenthal G. European macroseismic scale (1998) Cahiers du Centre Européen de Géodynamique et de Sismologie; 15:99.

Guzzetti F., C. A. (1999). Landslide hazard evaluation: a review of current techniques and their application in a multi-scale study, Central Italy. *Geomorphology* , Vol. 31, 181-216.

Hungr O., Leroueil S, Picarelli L (2014) The Varnes classification of landslide types. An upgrade. Landslide 11:167-194.

Jibson, R. H. (1998). A method forproducing digital probabilistic seismic landslide hazard maps: An example from the Los Angeles California area. *US Geol. Surv. Open-File Rep.* , 98-113.

Jibson, R. H. (2007). Regression models for estimating coseismic landslide displacement. *Eng. Geol. 91* , 209–218.

Kalkan E., Gülkan P., Yilmaz N., Çelebi M. (2009). Reassessment of Probabilistic Seismic Hazard in the Marmara Region. BSSA 99:2127-2146.

Kaynia A. M., S. E. (2011). Real-time mapping of earthquake-induced landslides. *Bull Earthquake Eng* , 955-973.

Mahdavifar, M. J. M. (2008). Real-Time Generation of Arias Intensity and Seismic Landslides. *JSEE* , 81-90.

Newmark, N. (1965). Effects of earthquakes on dams and embankments. . *Geotechnique 15,* , 139-159.

Özel O., Cranswick E., Meremonte M., Erdik M., Safak E. (2002). Site Effects in Avcilar, West of Istanbul, Turkey, from Strong- and Weak-Motion Data. Bulletin of the Seismological Society of America, 92(1): 499–508.

Ozmen B. (2004). Isoseismal Map of Izmit Earthquake. In: Izmit Körfezi Depremin in Hasar Durumu (Rakamsal Verilerle), damage in the Izmit Bay Earthquake (with quantitative data), Turkey DepremVakli, Istanbul.

Picozzi M., Strollo A., Parolai S., Durukal E., Özel O., Karabulut S., Zschau J., Erdik M. (2009). Site characterization by seismic noise in Istanbul,Turkey. Soil Dynamics and Earthquake Engineering, 29. 469-482.

Soeters R. V. W. (1996). Slope instability, recognition, analysis, and zonation. Turner A.K., Schuster R.L. ed. Landslide investigation and mitigation, Transport research council. , 129-177.

Varnes D.J. (1978). Slope movement types and processes. In: Schuster R.L. & Krizek R.J. (Eds.), Special Report 176 Landslides: Analysis and Control. Transportation Research Board, National Research Council, Washington D.C., 11-33.